Author Manuscript

Author Manuscript

Author Manuscript

Author Manuscript

HHS Public Access

Author manuscript

Cell Rep. Author manuscript; available in PMC 2019 December 26.

Published in final edited form as:

Cell Rep. 2019 April 02; 27(1): 238–254.e6. doi:10.1016/j.celrep.2019.03.009.

The Hematopoietic Oxidase NOX2 Regulates Self-Renewal of Leukemic Stem Cells

Biniam Adane[1,2,7], **Haobin Ye**[1], **Nabilah Khan**[1], **Shanshan Pei**[1], **Mohammad Minhajuddin**[1], **Brett M. Stevens**[1], **Courtney L. Jones**[1], **Angelo D'Alessandro**[2], **Julie A. Reisz**[2], **Vadym Zaberezhnyy**[2], **Maura Gasparetto**[1], **Tzu-Chieh Ho**[4], **Kathleen K. Kelly**[3], **Jason R. Myers**[4], **John M. Ashton**[4], **Julie Siegenthaler**[3], **Tsutomu Kume**[6], **Eric L. Campbell**[5], **Daniel A. Pollyea**[1], **Michael W. Becker**[4], **Craig T. Jordan**[1,8,*]

[1]Division of Hematology, Anschutz Medical Campus, University of Colorado, Aurora, CO 80045, USA

[2]Department of Biochemistry and Molecular Genetics, Anschutz Medical Campus, University of Colorado, Aurora, CO 80045, USA

[3]Department of Pediatrics, Anschutz Medical Campus, University of Colorado, Aurora, CO 80045, USA

[4]Genomics Research Center, University of Rochester, NY 14642, USA

[5]School of Medicine, Dentistry and Biomedical Sciences, Queens University, Belfast, UK

[6]Feinberg Cardiovascular and Renal Research Institute, Northwestern University School of Medicine, Chicago, IL 60611, USA

[7]Present address: Department of Pediatric Oncology, Dana-Farber Cancer Institute, Boston, MA 02215, USA

[8]Lead Contact

SUMMARY

The NADPH-dependent oxidase NOX2 is an important effector of immune cell function, and its activity has been linked to oncogenic signaling. Here, we describe a role for NOX2 in leukemia-initiating stem cell populations (LSCs). In a murine model of leukemia, suppression of NOX2

This is an open access article under the CC BY-NC-ND license (http://creativecommons.org/licenses/by-nc-nd/4.0/).

*Correspondence: craig.jordan@ucdenver.edu.

AUTHOR CONTRIBUTIONS

B.A. and C.T.J. conceived and designed all experiments, analyzed and interpreted the data, and wrote the manuscript. H.Y. assisted in designing experiments and manuscript preparation. N.K. and H.Y. assisted with all experiments involving murine models and xenograft studies. S.P. performed all bioinformatics analysis. M.M. assisted with lentivirus production for primary AML studies. B. M.S. organized animal protocols and assisted with flow cytometry analysis. C. L.J. performed metabolic analysis with help from A.D. and J.A.R. V.Z. performed irradiation and murine transplantation experiments. M.G. assisted with flow cytometry. T.-C.H. performed primary AML LSC transcriptomic studies. J.R.M. and J.M.A. performed Illumina sequencing and assisted with RNA-seq analysis. T.K., K.K., and J.S. generated and provided FOXC1$^{fl/fl}$ mice. E.L.C. provided NOX2 KO mice. D.A.P. and M.W.B. obtained AML patient specimens.

SUPPLEMENTAL INFORMATION

Supplemental Information can be found online at https://doi.org/10.1016/j.celrep.2019.03.009.

DECLARATION OF INTERESTS

The authors declare no competing interests.

Author Manuscript Author Manuscript Author Manuscript Author Manuscript

impaired core metabolism, attenuated disease development, and depleted functionally defined LSCs. Transcriptional analysis of purified LSCs revealed that deficiency of NOX2 collapses the self-renewal program and activates inflammatory and myeloid-differentiation-associated programs. Downstream of NOX2, we identified the forkhead transcription factor FOXC1 as a mediator of the phenotype. Notably, suppression of NOX2 or FOXC1 led to marked differentiation of leukemic blasts. In xenotransplantation models of primary human myeloid leukemia, suppression of either NOX2 or FOXC1 significantly attenuated disease development. Collectively, these findings position NOX2 as a critical regulator of malignant hematopoiesis and highlight the clinical potential of inhibiting NOX2 as a means to target LSCs.

Graphical Abstract

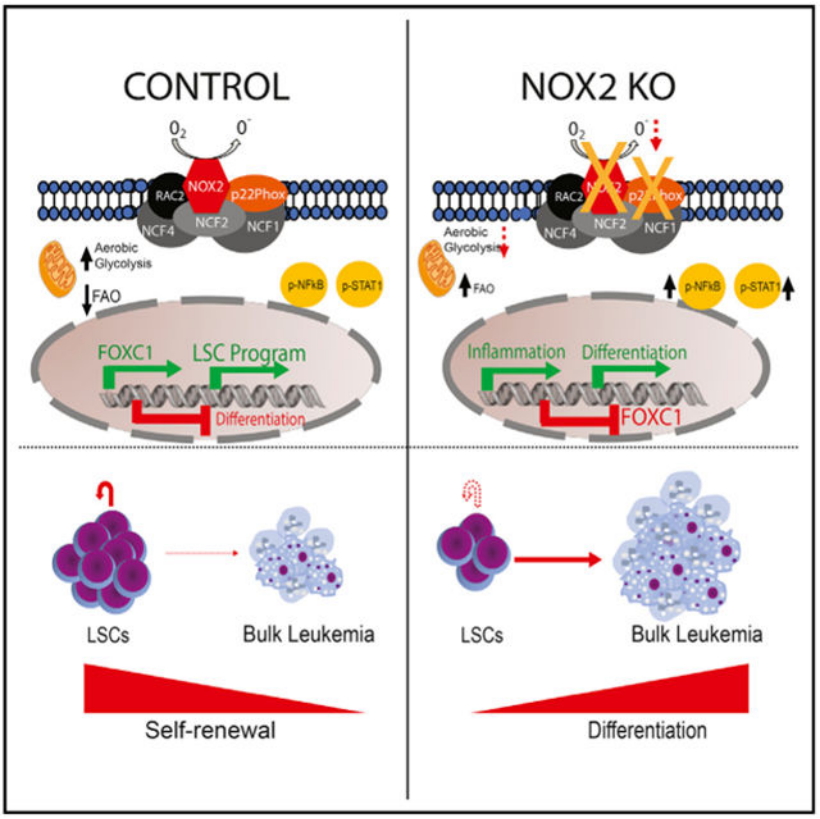

In Brief

The NADPH-dependent oxidase NOX2 is important for normal myeloid cell function. Adane et al. show that NOX2 is expressed in leukemic stem cells, where it regulates the balance of myeloid differentiation and self-renewal. Deficiency of NOX2 altered core metabolism, exacerbated inflammatory signaling, and limited *in vivo* disease development.

INTRODUCTION

Careful regulation of the balance between self-renewal and differentiation of hematopoietic stem cells (HSCs) is critical to ensure the proper function of the blood-forming system

Author Manuscript Author Manuscript Author Manuscript Author Manuscript

(Seita and Weissman, 2010). Subversion of molecular mechanisms that regulate these processes leads to defective immune functions and is often causally linked to the development of leukemia (He et al., 2009; Moran-Crusio et al., 2011; Shao et al., 2011). The ability to properly control cellular levels of reactive oxygen species is one of the best-understood factors that regulate the biology of stem cells. While excess amounts of reactive oxygen species (ROS) limit the function of HSCs (Ito et al., 2006; Tothova et al., 2007) at physiologic levels, ROS are required for the proper function of stem and progenitor cells (Juntilla et al., 2010; Morimoto et al., 2013; Owusu-Ansah and Banerjee, 2009). Therefore, careful modulation of ROS can play a programmatic role in stem cell quiescence and differentiation.

NADPH oxidases are a family of multimeric oxido-reductase enzymes that catalyze the production of superoxide anions. The holoenzyme is composed of a heterodimeric catalytic domain containing NOX1–NOX4 (in mice) and p22Phox, the cytosolic accessory factors (NCF1, NCF2, and NCF4), and the GTPase RAC proteins (Figure 1A). The hematopoietic version, NOX2, primarily functions in mature myeloid cells during the respiratory burst phase of phagocytosis (Groemping and Rittinger, 2005; Panday et al., 2015). Distinct from this function, NOX2 and its paralogs can produce physiologic levels of ROS and, in large part owing to their membrane proximal localization, can also modulate mitogenic signaling events to influence many aspects of cell biology (Jiang et al., 2011).

A number of studies have uncovered important functional roles for NADPH oxidases in several types of somatic stem cells. Spermatogonial stem cells derived from NOX1 knockout (KO) mice have aberrancies in their ability to self-renew (Morimoto et al., 2013). Similarly, NOX2 KO mice have defective neural stem cell function and impaired adult hippocampal progenitor proliferation (Dickinson et al., 2011; Le Belle et al., 2011). In the hematopoietic system, deficiency of either NOX2 or the GTPase RAC proteins significantly perturbs the normal balance of blood cell production and limits the self-renewal potential of HSCs (Cancelas et al., 2005; Roberts et al., 1999; Weisser et al., 2016; Yang et al., 2007). Moreover, loss-of-function mutations in genes encoding several subunits of the enzyme are causal for chronic granulomatous disease, a rare inherited immunodeficiency syndrome with an estimated frequency of 1/200,000 to 1/250,000 newborns (Giardino et al., 2017). A number of studies aimed at understanding the role of NADPH oxidases in the settings of malignant tumors have also uncovered some aspects of their function. In colorectal cancers, RAC1 stimulates ROS production from NADPH oxidase to facilitate WNT-signaling-driven intestinal progenitor cell expansion and transformation (Myant et al., 2013). In leukemic cells harboring driver mutations in tyrosine kinases, including BCR-ABL, JAK2, or $FLT3^{ITD}$, NADPH oxidases primarily potentiate oncogenic signaling to influence cell growth, migration, and metabolism (Grauers Wiktorin et al., 2018; Hole et al., 2013; Marlein et al., 2017; Moloney et al., 2017; Reddy et al., 2011). Moreover, RAC2-deficient BCR-ABL-transformed leukemic cells appear to have diminished leukemia-initiating potential upon transplantation (Sengupta et al., 2010). Collectively, these observations suggest that the NOX2 complex can play important biological functions in normal and malignant stem cells. Hence, in the present study using transgenic mice, a genetically defined murine model of myeloid leukemia, and xenograft studies of primary human-patient-derived leukemia specimens, we provide evidence supporting the importance of NOX2 in the pathogenesis of

Author Manuscript Author Manuscript Author Manuscript Author Manuscript

LSCs *in vivo*. We further elucidate the mechanisms operating downstream of NOX2 to regulate the function of leukemic stem cells.

RESULTS

The NOX2 Complex Is Expressed by Myeloid-Biased Multipotent Progenitors

To gain insight into the potential role of NOX2 in the normal biology of the blood-forming system, we initially performed qRT-PCR-based analyses of purified hematopoietic stem and progenitor cells (HSPCs) (LSK cells) and measured the mRNA expression levels of genes encoding all subunits of the complex (Figure 1A). Compared to all the other paralogs, NOX2 is expressed at significantly higher levels in HSPCs (Figure 1B). Importantly, all the accessory subunits of the enzyme complex are also sufficiently expressed (Figure S1A). Since LSKs are a mixed population composed of long-term self-renewing HSCs (LT-HSCs) and a number of multipotent progenitors (MPPs) (Pietras et al., 2015; Wilson et al., 2008), we next took advantage of a previously published genome-wide expression dataset to evaluate the relative abundance of multiple subunits of the NOX2 complex in highly purified populations (Cabezas-Wallscheid et al., 2014). Interestingly, at steady state, NOX2 levels are the highest in the myeloid-biased MPP2 and/or MPP3 subpopulations compared to LT-HSCs, MPP1s and the lymphoid biased MPP4 subpopulation (Figure 1C) (Cabezas-Wallscheid et al., 2014; Pietras et al., 2015) whereas the other subunits of the complex are expressed in nearly all subpopulations examined (Figure S1B). Furthermore, within the MPP3 compartment, NOX2 is the only paralog expressed (Figure 1D). Combined, these results support the interpretation that a myeloid-biased subset of HSPCs possess the full repertoire of NOX2 complex proteins, and thus, NADPH oxidase activity may have a unique functional role in these subpopulations.

NOX2-Deficient HSCs Have Myeloid-Biased Output and Regenerative Defects

To investigate the potential role of NOX2 in normal hematopoiesis, we next performed comparative phenotypic characterization of age- and sex-matched wild-type (WT) and transgenic NOX2-deficient (NOX2 KO) mice (Figure S1C) (Pollock et al., 1995). While total marrow cellularity is relatively comparable (Figure S1D), consistent with previous reports, NOX2 KO mice have expanded immunophenotypically defined HSPCs (Figure S1E) (Weisser et al., 2016). Interestingly, within HSPCs, only the myeloid biased MPP2 and/or MPP3 subsets, where we observed the highest expression of NOX2, show marked expansion, while the frequency of LT-HSCs, MPP1s, and MPP4s were virtually indistinguishable between the two genotypes (Figures 1E and 1F). In the peripheral blood (PB), differential cell counts revealed that NOX2 KO mice generally produce a larger number of leukocytes (Figure 1G). Most notably, much of the increase is due to the preferential overproduction of myeloid cells (Figures 1G, 1H, and S1F). In line with these findings, the bone marrow (BM) representation of CD11b- and MAC1-expressing myeloid cells was also increased in NOX2 KO mice (Figure 1I). Collectively, these findings suggest that at steady state, NOX2 functions to influence the magnitude of myelopoiesis starting at the earliest stage of multilineage differentiation.

Author Manuscript Author Manuscript Author Manuscript Author Manuscript

Given the observation that hematopoiesis is considerably perturbed in NOX2-deficient mice, we examined the extent to which HSC function is compromised in the absence of NOX2 by performing competitive repopulation assays. Analysis of engrafted mice revealed that NOX2-deficient HSCs are significantly limited in their ability to contribute to all lineages of hematopoiesis (Figures 1J and S1G). Moreover, analysis of BM showed that NOX2 KO mice also fail to regenerate and contribute to the LT-HSC and MPP compartments (Figure S1H). Taken together, these results strongly suggest that NOX2 controls the self-renewal potential of HSCs in the context of transplantation-induced regenerative stress.

Depletion of the NOX2 Complex Attenuates Leukemogenesis *In Vivo*

Leukemias often arise by the oncogenic transformation of normal HSPCs through corruption of self-renewal, proliferation, and differentiation mechanisms. Given our observations in normal hematopoietic cells that NOX2 deficiency perturbs myelopoiesis and limits self-renewal, we hypothesized that NOX2 could have a functional role in the biology of malignant myeloid leukemia-initiating stem cell populations (LSCs). To test the hypothesis, we utilized a genetically defined murine model of aggressive blast crisis myeloid leukemia induced by retroviral vectors carrying two potent oncogenic chromosomal translocations, BCR-ABL and NUP98-HOXA9, each independently marked by the fluorescent proteins GFP and YFP, respectively (Figure 2A) (Dash et al., 2002). In this model, we have previously characterized the immunophenotype (Sca1+ Lineage−) and several functional aspects of the LSC that drive and sustain the disease (Ashton et al., 2012; Neering et al., 2007; Ye et al., 2016). Using qRT-PCR-based analyses, we initially determined the relative expression levels of NADPH oxidase genes. Consistent with the normal HSPCs, the results showed that NOX2 is by far the predominant paralog expressed in leukemic stem cells (Figure S2A).

Next, to investigate the potential role of NOX2 in leukemia initiation and development, we transduced immature bone-marrow-derived hematopoietic cells from age- and sex-matched WT and NOX2 KO mice with our retroviral constructs and transplanted them into syngeneic recipient mice. BM cells from both genotypes were equally and efficiently transformed by the oncogenes (Figure S2B). Intriguingly, recipients of NOX2 KO leukemia have relatively lower disease burden in the BM and spleen compared to WT controls (Figures 2B, 2C, and S2C). Moreover, re-transplantation of purified bone-marrow-derived primary leukemia cells into secondary recipients resulted in further attenuation of disease development (Figures 2D and S2D). Cytospin preparations and histopathologic analysis also revealed reduced prevalence of leukemic cells in the PB and relatively subdued invasion of extramedullary tissues (Figures 2E, S2E, and S2F). Consistent with these findings, we observed marked extension of survival in mice engrafted with NOX2 KO leukemia, with the disease latency being significantly longer in recipients of secondary leukemia (Figure S2G). Finally, to evaluate the functional impact of NOX2 deficiency at the level of LSCs, we performed a limiting dilution analysis by transplanting a graded dose of LSCs into recipient mice. Our results revealed that the frequency of functionally defined leukemia stem cells is substantially lower in NOX2 KO leukemia cells relative to controls (Figure 2F).

Author Manuscript Author Manuscript Author Manuscript Author Manuscript

Since NOX2 is a multimeric complex, we next wanted to evaluate the broader requirement of the entire enzymatic complex. To this end, we investigated the role of p22Phox, a critical subunit of the complex that dimerizes with NOX2 to form the catalytically active enzyme. Using lentiviral short hairpin RNA (shRNA) constructs, we efficiently reduced the expression of p22Phox in primary BM-derived WT leukemia cells (Figure 2G). We then injected control and p22Phox knockdown (KD) cells into secondary hosts. Consistent with our findings using NOX2 KO leukemia, suppression of p22Phox also diminished the growth of leukemic cells in both the BM and spleen of transplanted mice (Figures 2H-2J). Taken together, these findings strongly argue that the NOX2 complex is expressed in LSCs and plays an important functional role in the engraftment, self-renewal, and proliferation of leukemic stem cells.

Deficiency of NOX2 Reduces Basal ROS and Impairs Core Metabolism

Since NOX2 produces reactive oxygen species as end products of catalysis, we measured the relative levels of ROS in leukemic explants from the BM of secondary recipient mice using the redox-sensitive fluorescent probe CellROX. We observe that NOX2 KO LSCs, as well as lineage-marker-expressing bulk leukemic cells, exist in a relatively reduced state (Figures 3A and 3B). Interestingly, non-leukemic cells co-inhabiting the BM niche also displayed reduced ROS, suggesting that in the absence of NOX2 the leukemic microenvironment is also less oxidized (Figure 3C). To directly test whether NOX2 contributes to physiologic levels of ROS, we next antagonized its enzymatic activity with small-molecule inhibitors (Altenhöfer et al., 2015). Inhibition of NOX2 reduced intracellular ROS levels relative to controls, suggesting that NOX2 partially contributes to the overall redox state of leukemic cells (Figures S3A and S3B). Given these observations, we decided to investigate whether general oxidative-stress-associated mechanisms contribute to the phenotypes observed in NOX2 KO leukemia cells. To this end, we treated a cohort of mice engrafted with WT leukemia with the universal ROS scavenger N-acetyl cysteine (NAC) throughout the course of disease development (Figure S3C). NAC treatment marginally reduced ROS levels in the BM of recipient mice (Figure S3D). Importantly however, we did not observe a significant attenuation of disease progression *in vivo* (Figure S3E), suggesting that overt oxidative-stress-linked mechanisms have a limited effect on leukemogenesis in this model.

Since the substrates for NOX2, namely molecular oxygen and the cofactor NADPH, are critical components of several cellular metabolic pathways, we next investigated the impact of NOX2 deficiency in the core metabolism of leukemia cells. Mitochondrial oxygen consumption and glycolytic flux measurements were carried out on BM-derived lineage-negative WT and NOX2 KO leukemia cells. Interestingly, relatively reduced oxygen consumption and significantly diminished maximal mitochondrial respiratory capacity were observed in NOX2 KO leukemia cells (Figures 3D and 3E). Moreover, measurement of the rate of extracellular acidification (ECAR) as an indicator of glycolytic potential revealed that NOX2 KO leukemia cells utilize glycolysis to a surprisingly limited degree (Figure 3F). Notably, in NOX2 KO leukemia cells, both mitochondrial and glycolytic metabolism were relatively less dynamic, as there was a blunted response to chemical perturbation of the electron transport chain or proton conductance across mitochondrial membrane. Combined,

Author Manuscript Author Manuscript Author Manuscript Author Manuscript

these findings suggest that there is a marked impairment of core metabolic pathways in leukemic cells in the absence of NOX2.

To gain a better insight into the metabolic reprograming induced by lack of NOX2, we performed global metabolic profiling using ultra-high-pressure liquid chromatography-coupled mass spectrometry (UHPLC-MS). Principal-component analysis showed that WT and NOX2 KO leukemic cells segregated based on their metabolic profiles (Figure S3F), indicating potentially distinct modes of metabolism. Consistent with their reduced state, NOX2 KO leukemia cells contained elevated levels of the antioxidants ascorbate, glutathione, and the glutathione precursor dipeptide cysteine-glycine (Figure S3G). Most importantly, a closer examination of the identity of the differentially abundant metabolites revealed that NOX2 KO leukemic cells contain high levels of carnitine-conjugated short- and intermediate-length free fatty acids (Figures 3G, 3H, and S3H). Carnitine conjugation facilitates the activation and transport of free fatty acids into the mitochondria for oxidation. Thus, we next measured the relative rate of fatty acid oxidation (FAO) using tritium-labeled palmitate. The results showed that NOX2 KO leukemia cells have a substantially higher rate of FAO than WT controls (Figure 3I). In totality, these findings suggest that depletion of NOX2 rewires key metabolic pathways promoting the use of fatty acids as mitochondrial fuel and limiting glycolytic pathways that generate essential metabolites for anabolic reactions that leukemia cells use to grow and proliferate.

Deficiency of NOX2 Abrogates Stem Cell-Associated Transcriptional Programs

To further understand the potential mechanisms by which NOX2 regulates leukemogenesis, we assessed the impact of NOX2 loss on global transcriptional output. We purified LSCs from BM explants of secondary recipients and performed RNA sequencing (RNA-seq) analysis. Unsupervised hierarchical clustering segregated the samples into their respective genotypes (Figure S4A). To uncover the NOX2-mediated gene expression changes, we applied stringent statistical criteria to identify a total of 143 differentially expressed genes, of which 80 were upregulated (log2 fold change > 1.5, $p < 0.05$) and 63 were downregulated (log2 fold change < −1.5, $p < 0.05$) in NOX2 KO LSCs compared to WT controls (Table S1). Among genes that are highly increased in expression in NOX2 KO LSCs, several of them are associated with mature myeloid cell function. These include the myeloid transcription factor *CEBPε*, a number of proteolytic enzymes, including the neutrophil elastase (*Elane*), and Cathepsin G (*CTSG*), Cathepsin S (*CTSS*), as well as the inflammatory amplifier proteins *S100a8* and *S100a9* (Figure 4A). Conversely, several genes encoding cell adhesion (*ITGb3*, *Tie1*, and *CD96*) and signaling adaptor molecules (*GRB7* and *STAP2*), as well as the stem cell associated transcription factor *FOXC1* and the retinol metabolizing dehydrogenase *ALDH1a2*, were downregulated in NOX2 KO LSCs relative to WT controls (Figure 4A). We validated some of these observations using qRT-PCR-based analysis of gene expression on LSCs purified from an independent cohort of WT and NOX2 KO leukemia as well as from control and p22Phox KD leukemic cells (Figures 4B and 4C).

Next, to gain deeper insight into the global genetic changes that are brought about by the lack of NOX2 in leukemic stem cells, we performed gene set enrichment analysis (GSEA). Consistent with our metabolic analysis, we observed depletion of genes involved in

Author Manuscript Author Manuscript Author Manuscript Author Manuscript

glycolysis and glucose metabolism and enrichment of fatty-acid-metabolism-associated genes in NOX2 KO LSCs relative to WT controls (Figures S4B and S4C). Strikingly, gene expression signatures associated with both normal HSCs (Chambers et al., 2007) and leukemia stem cells (Gal et al., 2006) were markedly enriched in WT LSCs relative to their NOX2 KO counterparts (Figure 4D). Conversely, genes that are selectively depleted in LSCs (Gal et al., 2006) as well as a gene set signature of leukocyte differentiation were highly enriched in NOX2 KO LSCs relative to controls (Figure 4E). Moreover, we also observed a marked enrichment of innate immune system related pathways in NOX2 KO LSCs (Figure S4D). Taken together, the data strongly suggests that NOX2 plays an important role in maintaining stem cell associated programs in LSCs and in its absence leukemic cells display enhanced proclivity to activate transcriptional programs akin to those employed by functionally specialized mature myeloid cells.

Deficiency of NOX2 Induces the Differentiation of Leukemic Cells

Given the loss of stem cell potential and the corresponding induction of myeloid-maturation-related genetic programs, we next examined whether leukemic cells undergo terminal differentiation as a consequence of NOX2 loss. Immunophenotypic characterization was performed on secondary leukemic explants from the BM of recipients of WT and NOX2 KO leukemia. We observed a significant increase in the fraction of leukemic cells expressing canonical myeloid maturation markers in the absence of NOX2 relative to controls (Figure 4F). In addition, histologic analysis via May-Grünwald-Giemsa staining showed that NOX2 KO leukemia cells display morphologic characteristics of myeloid differentiation marked by segmented nuclei, increased abundance of granular and vacuolar structures, and enlarged cytoplasms (Figures 4G and S4F). Similar observations were also made in p22Phox KD leukemia cells relative to controls (Figures 4H, 4I, and S4G). Therefore, the combined results of our studies suggest that the NADPH oxidase complex promotes the extensive self-renewal potential of leukemic stem cells and underscores an underlying defect in transcriptional programs essential for maintaining leukemic stem cells in an undifferentiated state in the absence of NOX2.

NOX2 Controls Inflammatory Signaling Pathways

Next, we focused on cell signaling pathways that are dysregulated in NOX2 KO leukemia cells with the aim of discerning some of the molecular mechanisms involved in the aberrant transcriptional rewiring. GSEA identified several inflammatory signaling pathways as being significantly induced in NOX2 KO LSCs relative to controls. These include general cytokine_cytokine_receptor, interleukin-17 (IL-17)-mediated signaling, Toll-like receptor signaling, janus kinase signal transducer and activator of transcription (JAK-STAT) signaling pathways, and NF-κB target genes, which were all highly enriched in NOX2 KO LSCs relative to WT controls (Figures 5A-5C and S5A). To confirm these findings, we evaluated the activation state of components of the NF-κB and JAK-STAT signaling pathways. Immunoblot analysis revealed that, at steady state, NOX2 KO leukemia cells have higher levels of phosphorylated NF-κB and STAT1 (Figure 5D). Intriguingly, we also observed increased activation of the stress responsive kinase p38 MAPK as well as its downstream effector transcription factor, JUN-c, in NOX2 KO leukemia cells (Figures 5E and 5F). To understand whether NOX2 has an impact on the ways leukemic cells respond to

Author Manuscript Author Manuscript Author Manuscript Author Manuscript

inflammatory stimuli, we treated WT and NOX2 KO cells with tumor necrosis factor alpha (TNF-α) *in vitro*. Interestingly, in WT leukemia cells, TNF-α stimulation produced a feedback inhibitory effect and reduced the activation of inflammatory and stress signaling pathways. In sharp contrast, NOX2 KO leukemia cells displayed a severely blunted feedback inhibitory capacity (Figures 5D-5F). Consistent with these findings, *in vitro* treatment with TNF-α or Toll-like receptor agonists resulted in a greater, dose-dependent apoptotic cell death in NOX2 KO leukemia cells compared to WT controls (Figures 5G and S5B). Thus, NOX2 KO leukemia cells fail to properly regulate inflammatory cell signaling and as a result exist in a hyperinflammatory state and experience chronic cellular stress, which combined compromises their leukemogenic potential.

The Forkhead Transcription Factor FOXC1 Regulates Leukemogenesis Downstream of NOX2

Our transcriptional, cell signaling, immunophenotypic, and morphologic analysis led us to propose that deficiency of NOX2 reprograms key transcriptional networks and forces the differentiation of leukemic blasts. Thus, a fundamental question is whether transcription factors whose expression is misregulated as a consequence of NOX2 deficiency could be responsible for reversing the developmental arrest enforced by the leukemogenic oncogenes. To investigate this, we queried the list of genes upregulated or repressed in NOX2 KO LSCs and identified candidate transcription factors. Among the transcription factors whose expression is altered, the forkhead family member *FOXC1* showed one of the highest-fold repressions, whereas the important myeloid differentiation factor *CEBPε* was among the most significantly upregulated transcription factor in NOX2 KO LSCs (Table S1; Figure 4A). Therefore, we evaluated the relative expression levels of these two transcription factors in the different subpopulation of leukemic cells as well as normal hematopoietic precursors. *FOXC1* expression is selectively induced in leukemic stem cells relative to several primitive normal hematopoietic cells, suggesting a leukemia specific function. In addition, *CEBPε* is also relatively higher in LSCs than in normal undifferentiated hematopoietic cells, reflecting the myeloid identity of the leukemia cells (Figure S6A). Most importantly, *FOXC1* expression is the highest in the LSC compartment relative to the bulk of leukemic cells, whereas *CEBPε* is predominantly expressed in lineage-marker-expressing differentiated leukemic cells (Figure 6A). Therefore, we hypothesized that in leukemic stem cells, FOXC1 represses myeloid differentiation downstream of NOX2, partly through silencing of myeloid-lineage-instructive transcriptional programs.

To directly investigate the role of FOXC1 in leukemic stem cells, we utilized transgenic mice expressing a floxed allele of endogenous FOXC1 and a td-Tomato Cre reporter knocked into the Rosa26 locus (Figures S6B and S6C). We generated primary leukemia in the FOXC1 floxed background and introduced tamoxifen-inducible Cre recombinase to assess the impact of conditional deletion of FOXC1 (Figure 6B). Treatment of leukemic cells with the synthetic estrogen receptor agonist 4-hydroxy tamoxifen (4OHT) led to induction of the reporter and resulted in efficient depletion of *FOXC1* mRNA as well as protein levels (Figures 6C, 6D, and S6D). Moreover, we observed that deletion of FOXC1 robustly activates *CEBPε* as well as its known downstream target *Elane* and a number of

Author Manuscript Author Manuscript Author Manuscript Author Manuscript

mature myeloid cell-specific transcripts similar to what we had observed in NOX2 KO and p22Phox KD LSCs (Figure 6D).

To evaluate the functional role of FOXC1 in the *in vivo* development of leukemia, we transplanted control and FOXC1-deleted leukemia cells into recipients. Compared to controls, mice transplanted with FOXC1-deleted leukemia cells have significantly lower disease burden and survived relatively longer (Figures 6E, 6F, and S6E). Limiting dilution analysis also revealed that FOXC1-deleted leukemic cells have a marked reduction in the frequency of functionally defined LSCs (Figure 6G). Moreover, transplantation of leukemic cells and the subsequent deletion of FOXC1 after engraftment also significantly compromised disease development, suggesting that FOXC1 is crucial for the engraftment, propagation, and maintenance of leukemic stem cells *in vivo* (Figures S6F and S6G). Finally, to investigate whether FOXC1 contributes to the developmental arrest of leukemic blasts, we evaluated the immunophenotypic and histologic features of leukemic cells explanted from recipients of control and FOXC1-deleted leukemia. Our results showed marked induction of myeloid-maturation-associated surface antigens and morphologic changes indicative of differentiation (Figures 6H, 6I, and S6H). Collectively, these results argue that FOXC1 is part of the oncogenic transcriptional program operating downstream of NOX2 that limits the developmental potential of leukemic stem cells by shutting off myeloid-lineage-specific genetic programs.

NOX2 Is Expressed in Primary Human AMLs, and Its Suppression Induces Cell Death and Differentiation

Our studies in the genetically defined murine model revealed that NOX2 is critical for the development and maintenance of leukemic stem cells. We next wanted to assess the extent to which NOX2 is involved in the biology of human acute myeloid leukemia. In order to begin to understand its role, we first evaluated the expression levels of all NADPH-oxidase-related genes, including the accessory subunits that make up the enzymatic complex, as well as other related oxido-reductase enzymes from the acute myeloid leukemia (AML) dataset of The Cancer Genome Atlas (TCGA) project. NOX2 is by far the predominant oxidase expressed in AML cells relative to all the other paralogs and related enzymes (Figure 7A). Moreover, all the necessary subunits are also sufficiently expressed in leukemic cells. Since the TCGA data were generated from the transcriptome of unfractionated bulk leukemic cells, we next assessed the expression of NOX2 in functionally defined leukemia stem cells (Ho et al., 2016). In multiple diagnostic specimens of primary human LSCs, we observed a substantial enrichment of NOX2 transcripts relative to all other family members (Figures 7B and S7A). Correspondingly, we also observed a similarly high level of expression for all accessory subunits of the complex, suggesting that human leukemic stem cells are equipped with the full repertoire of the NOX2 complex.

To study the potential cell-autonomous role of NOX2 in primary human AML cells, we depleted its expression *in vitro* using lentiviral vectors expressing shRNA constructs. Next, we plated equal numbers of control and NOX2 KD primary AML cells in the presence of supportive cytokines (IL-3, stem cell factor [SCF], and FL3) and followed the *in vitro* expansion over an extended period of time. Interestingly, suppression of NOX2 significantly

Author Manuscript Author Manuscript Author Manuscript Author Manuscript

attenuated the *in vitro* expansion of leukemic cells relative to controls (Figure 7C). Consistent with these observations, NOX2 KD cells undergo an increased level of apoptotic cell death relative to controls (Figures 7D and S7B). In addition, treatment with the pan-NADPH oxidase inhibitor diphenyliodonium (DPI) also led to significantly reduced viability of leukemic cells, suggesting that NOX2 potentiates the survival and proliferation of primary human leukemia cells under *in vitro* culture conditions (Figure S7C).

Based on the findings from our studies using the murine model, we hypothesized that NOX2 may also regulate myeloid differentiation. qRT-PCR-based analysis of gene expression revealed that compared to non-targeted shRNA controls, NOX2 KD AML cells consistently upregulated the myeloid differentiation transcription factor *CEBPε* as well as the proteolytic enzymes *Elane* and *CTSG* transcripts (Figures 7E and S7D). More importantly, NOX2 KD AML cells also displayed immunophenotypic and morphologic signs of myeloid differentiation (Figures 7F, 7G, and S7E). Combined, our results show that NOX2 controls critical transcriptional programs that mediate the survival and maintenance of human AML cells in the undifferentiated state.

Suppression of NOX2 Limits the Xenograft Potential of Primary Human Leukemia Cells

Given the observed effect of *in vitro* modulation of NOX2 combined with its expression in functionally defined leukemic stem cells, we hypothesized that NOX2 could potentially have a functional role in human LSCs. Thus, we performed xenograft experiments using patient-derived primary human AML and blast crisis chronic myeloid leukemia (CML) specimens to evaluate the extent to which leukemic cells engraft and expand *in vivo* after transduction with lentiviral vectors expressing shRNAs against NOX2. Notably, the percentage of successfully transduced, GFP+ leukemic cells was comparable across experimental groups before transplantation (Figures S7F and S7G). However, after 8–12 weeks of engraftment, the fraction of total GFP+ cells as well as the relative engraftment level of the KD leukemic cells was significantly limited relative to the controls in all specimens evaluated (Figures 7H-7K, S7F, and S7G). Therefore, NOX2 plays important functional role in the engraftment, maintenance, and expansion of human primary LSCs.

FOXC1 Is Expressed in a Subset of Primary Human AMLs and Regulates Leukemogenesis *In Vivo*

Our data in the murine model showed that the forkhead family transcription factor FOXC1 constitutes part of the transcriptional program operating downstream of NOX2 to regulate the function of leukemic stem cells. Therefore, we next asked whether FOXC1 is expressed in immunophenotypically defined primitive subpopulation of human leukemia specimens. To this end, we purified the $CD34^+$ fraction of leukemic cells from several patient-derived specimens as well as normal cord blood and mobilized adult BM mononuclear cells and performed qRT-PCR-based gene expression analysis. FOXC1 expression is minimal in normal hematopoietic precursors and the majority of leukemic specimens. However, consistent with previous reports, leukemias harboring mixed lineage leukemia (MLL) rearrangement or the translocation t(6:9) expressed high levels of FOXC1 transcripts (Figure S7H; Table S2) (Somerville et al., 2015). To test whether the expression of FOXC1 is under the control of NOX2 in these specimens, we purified $CD34^+$ cells and transduced with

Author Manuscript Author Manuscript Author Manuscript Author Manuscript

lentiviral shRNA constructs targeting NOX2. Suppression of NOX2 reduced the expression of *FOXC1* transcript levels (Figure S7I). Therefore, in at least a subset of human primary AMLs, NOX2 modulates the expression of FOXC1 at the transcriptional level. Finally, to determine whether FOXC1 regulates the function of leukemia stem cells *in vivo*, we knocked down FOXC1 in a blast crisis CML specimen and two AML specimens with high expression of FOXC1 and transplanted immunocompromised recipient mice. Suppression of FOXC1 resulted in severely attenuated engraftment of recipient mice, suggesting that FOXC1 plays key functional role in promoting the growth and maintenance of primary human LSCs (Figures 7L-7O, S7J, and S7K).

DISCUSSION

Myeloid leukemias arise from hematopoietic precursors through corruption of genetic programs controlling proliferation, self-renewal, and myeloid lineage differentiation. Leukemia-initiating oncogenes often amplify stem cell-associated transcriptional programs and/or move them outside of their developmental context to induce a malignant state characterized by the accumulation of undifferentiated precursor cells. Hence, myeloid leukemias can be viewed as hematologic developmental disorders underwritten by aberrant myeloid cell production. Understanding the molecular mechanisms that are either collaborating with oncogenic programs or suppressed to permit the transformation of HSPCs and maintenance of leukemia stem cells is critical in order to design improved therapeutic approaches.

Previous studies have shown that deficiency of the hematopoietic oxidase NOX2 causes the expansion of HSPCs and the overproduction of myeloid cells (Weisser et al., 2016). We confirmed these findings and also show that NOX2 KO mice have marked increase in mature myeloid cells in the BM and PB, suggesting that NOX2 impacts the overall magnitude and balance of myelopoiesis. Enhanced myelopoiesis is frequently observed during infection-induced acute inflammation, wherein hematopoiesis is reconfigured to meet the demand generated by the active consumption of mature effector myeloid cells (Takizawa et al., 2017). In light of the hyper-inflammatory state of NOX2 KO mice, the enhanced myelopoiesis is thus in part a reflection of the lineage instructive effect of inflammation. Importantly however, here we provide evidence to show that NOX2 deficiency might also have an additional, cell-intrinsic contribution to the aberrant hematopoiesis observed in NOX2 KO mice. In support of this notion, we found that in WT mice under steady-state conditions, NOX2 expression is most evident in the myeloid-biased MPP2 and/or MPP3 subpopulations. Strikingly, coincident with this expression pattern, MPP2 and/or MPP3 subpopulations are the earliest developmentally defined hematopoietic cells that show significant expansion in NOX2-deficient mice.

We also observed defects of NOX2 KO BM cells in competitive repopulation studies, suggesting a potential cell-autonomous role for NOX2 under regenerative settings. Previous studies using hematopoietic specific KO of the GTPase RAC2 (an important subunit of the NOX2 complex) have also shown similar phenotypes, including expansion of hematopoietic precursors and cell-intrinsic regenerative defects (Cancelas et al., 2005; Roberts et al., 1999; Yang et al., 2007), further underscoring the potential cell-autonomous role of the NOX2

Author Manuscript Author Manuscript Author Manuscript Author Manuscript

complex in HSPCs. The exact mechanism by which the NOX2 complex impacts hematopoiesis is currently unclear. The mechanism likely involves a complex interplay between cell-autonomous signaling, heterotypic interactions with the niche, and the influence of cell-extrinsic inflammatory cues. Therefore, further analysis using conditional alleles of NOX2 is warranted to elucidate the underlying mechanism and parse out the relative contribution of each to the overall phenotype.

Suppression of NOX2 in a genetically defined aggressive murine model of blast crisis leukemia led to marked attenuation of disease development *in vivo*. Consistent with the well-characterized role of NOX2 in redox biology, we observed overall reductions in the level of ROS in leukemic cells lacking NOX2. However, our studies revealed that oxidative-stress-related mechanisms are minimally involved in the leukemic phenotype. Intriguingly, metabolic characterizations revealed deep impairments in both glycolytic and mitochondrial metabolism of leukemic cells in the absence of NOX2. Broadly speaking, deficiency of NOX2 favored fatty-acid-oxidation-dependent catabolism at the expense of glycolytic metabolism. The exact mechanism linking NOX2 to changes in tumor metabolism needs further investigation. Notably, previous reports have shown that in activated neutrophils, suppression of NOX2 negatively affects the rate of glycolysis, and under glucose-restricted conditions, immature neutrophils can burn fatty acids in the mitochondria to sustain NADPH-dependent ROS production (Baillet et al., 2017; Griffiths et al., 2017). These findings support the notion that NADPH oxidase can regulate core metabolic pathways in myeloid precursor cells. Spin-off reactions utilizing glycolytic intermediates provide substrates for building large macromolecules necessary for cell growth and therefore NOX2 deficiency likely engenders a metabolic state less adapted to the requirements of a highly proliferative tumorigenic state (Lunt and Vander Heiden, 2011).

Lack of NOX2 effectively collapsed stem cell-associated genetic programs, depleted functionally defined LSCs, and reversed the oncogene-induced developmental arrest, allowing leukemic stem cells to progress to a more mature state mirroring normal myelopoiesis. Gene expression and biochemical studies showed that aberrant, hyperinflammatory signaling dominates the cellular state of NOX2 KO LSCs. Together with the enhanced myelopoiesis and the hyperinflammatory state observed in non-leukemic NOX2 KO BM HSPCs, it is tempting to speculate that deficiency of NOX2 intrinsically promotes inflammatory signaling and myeloid differentiation in both malignant and non-malignant settings. Downstream of NOX2, we identified the forkhead family member transcription factor FOXC1 as part of the mechanism through which the transcriptional program of LSCs is maintained. FOXC1 is a critical regulator of early mesodermal development as well as the function of a number of somatic stem cells (Lay et al., 2016; Wang et al., 2016; Wilm et al., 2004). In the hematopoietic system, FOXC1 is expressed not in HSPCs but rather in reticular mesenchymal cells in the BM niche, and its deletion leads to profound defects in HSC function (Omatsu et al., 2014). Surprisingly, however, it was recently shown that FOXC1 is ectopically activated outside of its developmental context in a subset of human AMLs, and its expression is predominantly associated with the expression of the HOXA and/or HOXB locus (Somerville et al., 2015). Notably, leukemic cells in our murine model harbor the NUP98-HOXA9 translocation, which has previously been shown to activate the HOXA locus (Shima et al., 2017). Importantly, our findings here show that

Author Manuscript Author Manuscript Author Manuscript Author Manuscript

the expression of FOXC1 can be mediated by the activity of the NOX2 complex. Indeed, suppression of either NOX2 or p22Phox markedly reduced the expression of FOXC1.

In our model, FOXC1 is highly enriched in leukemic stem cells relative to the bulk leukemia cells and normal HSPCs. Studies in basal-like breast cancers have also shown that FOXC1 controls cancer stem cell properties (Han et al., 2015). Coupled with its function in mesodermal development and somatic stem cells, these data suggest that FOXC1 broadly maintains a stem cell genetic program under a multitude of contexts. Genetic deletion of FOXC1 led to the induction of myeloid differentiation. Notably, when compared to the differentiation induced by the suppression of components of the NADPH oxidase complex, which resulted in the accumulation of cells with morphologic features of granulocytic and monocytic cells, deletion of FOXC1 resulted primarily in monocytic differentiation, suggesting that it accounts for part of the mechanism downstream of NOX2. This finding is consistent with previous reports showing the role of FOXC1 in monocytic differentiation in AML.

Using the publicly available TCGA dataset and our own patient samples, we show that NOX2 is the predominant oxidase expressed in both bulk primary human AML cells and leukemic stem cells. Similarly, we also showed that FOXC1 is highly expressed in a subset of AMLs containing the leukemogenic translocations t(6:9) and t(11:16) encoding NUP214-DEK and MLL-CBP, respectively. A recent study has shown that FOXC1 expression is strongly associated with t(6:9) and the expression of the HOXA and/or HOXB locus, which is known to be activated in MLL-rearranged leukemia (Somerville et al., 2015). Genetic suppression of NOX2 in cultured primary human AML cells reduced the expression of FOXC1, induced the expression of mature myeloid cell-function-associated transcripts, and led to terminal differentiation. More importantly, shRNA-mediated suppression of either NOX2 or FOXC1 substantially attenuated the engraftment potential of primary human leukemia specimens into immunocompromised mice. From a clinical point of view, our findings suggest that inhibition of NOX2 could potentially serve as a viable therapeutic approach to induce differentiation of leukemic stem cells. NADPH oxidases are multimeric enzymes that utilize cofactors and require complex interactions between subunits for their function, thereby providing numerous opportunities to design inhibitory molecular agents. Indeed, ongoing clinical trials are evaluating small-molecule inhibitors of NADPH oxidases for various diseases.

STAR★METHODS

CONTACT FOR REAGENT AND RESOURCE SHARING

Further information and requests for resources and reagents should be directed to and will be fulfilled by the Lead Contact, Craig T. Jordan (Craig.jordan@ucdenver.edu).

EXPERIMENTAL MODEL AND SUBJECT DETAILS

MICE—Mice were housed in a pathogen free facility with strict adherence to The Recommended Guide for Care and Use of Laboratory Animals issued by the National Institutes of Health and animal protocols approved by the Institutional Animal Care and Use

Author Manuscript Author Manuscript Author Manuscript Author Manuscript

Committee at The University of Colorado school of medicine (IACUC). In each experiment, age of mice was balanced with maximum 2 weeks of difference between the experimental and control group.

FOXC1 F/F AI14-FLOX MICE—Heterozygous *Foxc1-flox* (Sasman et al., 2012); *Ai14-flox* (Jackson Laboratory stock number 007914) animals were crossed to generate Foxc1 floxed animals for this study.

PRIMARY AML XENOGRAFT STUDIES—NOD.Cg-*Prkdc*^{scid} *Il2rg*^{tm1Wjl} Tg(CMV-IL3,CSF2,KITLG)1Eav/MloySzJ(NSGS) mice originally purchased from Jackson laboratory (stock number 013062) and subsequently bred at the university of Colorado school of medicine animal facility, were conditioned 24 hours prior to transplant with 25 mg/kg busulfan via intra-peritoneal (IP) injection. Primary AML cells were infected with shRNA lentivirus 24 hours prior to transplant and injected via tail vein at a concentration of 2.0 e6 cells in 0.1ml saline per recipient mouse. A small fraction of the infection reaction is kept for additional 24 hours to determine the transduction efficiency. For all experiments, 8-12 mice were injected per experimental group. Engrafted mice were sacrificed after 8-12 weeks at which point, we typically observed > 15% leukemia in the BM.

PRIMARY HUMAN LEUKEMIA SPECIMENS—Primary human AML specimens were obtained from apheresis product, PB, or BM of AML patients who gave informed consent for sample procurement on the University of Colorado tissue procurement protocols. See Table S2 for additional details regarding sex, age and disease relevant information on human specimens used in the current study. The selection of particular specimens is based solely on the amenability of the samples for experimental procedures including *in vitro* culture studies, lentiviral infection and engraftment into immune compromised mice.

PRIMARY AML CELL CULTURE AND MEDIA—Primary human AML cells were resuspended at about 100-200 e6 cells per ml in freezing media composed of 50% FBS (GE Healthcare), 10% DMSO (Sigma) and 40% IMDM media (GIBCO) and then cryo-preserved in liquid nitrogen. Cells were thawed in 37°C water bath, washed twice in thawing media composed of IMDM (GIBCO), 2.5% FBS (GE Healthcare) and 10 ug/ml DNase (Sigma). Cells were cultured in base (IMDM+10%FBS) or cytokine supplemented media (IMDM, 10%FBS, 10ng/ml of IL3, SCF & FL3 from PeproTech) in 37C, 5% CO2 incubator.

HUMAN CORD BLOOD SAMPLES—Cord blood was obtained from healthy full-term pregnancies after informed consent in accordance with the Declaration of Helsinki from University of Colorado Hospital at Aurora. Initially, cord blood volume and cell counts were measured and then diluted 1:1 with PBS+ 2mM EDTA+0.5% BSA. Maximum 30 mL of diluted cord blood was carefully layered on 15 mL of Ficoll Paque in a 50ml falcon tube and centrifuged for 20 minutes, 800 g, without brakes. Middle (buffy coat) layer containing mononuclear cells was harvested and diluted 1:1 with PBS 2mM EDTA 0.5% BSA and then centrifuged for 5 minutes at 800 g. Cell pellets were collected and washed with PBS 2mM EDTA 0.5% BSA and centrifuged for 10 minutes at 200 g. Immunomagnetic labeling and separation were performed according to the manufacturer's manual of the CD34 MicroBead

Author Manuscript Author Manuscript Author Manuscript Author Manuscript

Kit, human (Miltenyi Biotec). Cells were either used immediately for experiments or frozen in Cryostor CS10.

CELL LINES—293FT and the 293 derivative Platinum-E cells were cultured in DMEM +1% P/S + 10% heat-inactivated FCS and used for lentiviral and retroviral packaging respectively.

METHOD DETAILS

BM cell isolation—Mice were euthanized by CO_2 asphyxiation followed by cervical dislocation. Tibia and femur bones were isolated and kept in ice-cold FACS buffer (DPBS, 2% heat inactivated fetal bovine serum). BM was flushed out using 1ml syringe fitted with 26G needle directly into 2mls of ice-cold FACS buffer in a FACS tube. BM clumps were broken up by pipetting repeatedly and centrifuged briefly. Cell pellets were re-suspended in 1 mL of 1 × RBC lysis buffer and centrifuged for 2 minutes. RBC lysed cell pellets were washed ones with FACS buffer, resuspended in 2mls of FACS buffer and passed through filter cap fitted FACS tubes (BD Bioscience). An aliquot of this single cell suspension was used for flow cytometric analysis.

PB isolation—100-200ul of PB was collected from mice directly into heparin-coated collection tubes by small puncture of the submandibular plexus vein with a 26 Gauge needle. Unclotted blood was transferred into 1.5 mL Eppendorf microfuge tubes containing 300ul of a 1:1 volume mixture of 2% dextran and Heparin sulfate solution. The mixture was vortexed and allowed to settle for 20 minutes. The upper, relatively clear layer containing mononuclear cells was transferred into narrow bottom FACS tubes and washed ones with 1 mL of ice-cold FACS buffer. Cells were RBC lysed as described above and washed one more time with FACS buffer before use for staining and flow cytometric analysis.

PB differential cell count—20ul of uncoagulated PB was allowed to migrate into capillary tubes, which were then inserted into the chamber of the HemaTrue differential cell count analyzer (HESKA). Three independent measurements were taken for each mouse and the average count was reported.

Flow Cytometric Analysis and Cell Sorting—BM and PB cells were stained with the appropriate antibodies (See key resources table above) for 30 minutes on ice in FACS buffer. Details of antibody combinations used to identify each population are given in the figure legends. After staining, cells were washed ones with ice-cold FACS buffer. Dead cells and cellular debris were excluded from the analysis using 4,6, diamino-2-phenylidole (DAPI) staining. A FACSAria II (BD) instrument was used for analysis and cell sorting. Cell purity was checked after each sort and generally ranged 96%–100%. Flow Cytometry data was visualized during collection via FACS Diva software (BD) and subsequently analyzed using FlowJo10 software.

RT-QPCR Analysis—Cells collected from the sorter were washed ones with ice-cold FACS buffer and either used immediately or flash frozen and subsequently used for RNA extraction. RNA from small number of cells was isolated using the RNeasy Micro kit

Author Manuscript Author Manuscript Author Manuscript Author Manuscript

(QIAGEN) following the manufacturers instruction. On column Dnase digestion was performed to eliminate contamination with genomic DNA. RNA was quantified using Nanodrop spectrophotometer (Fisher Thermo scientific) and was subsequently revers transcribed into cDNA using the qScript cDNA synthesis kit (QuantaBio). cDNA was ultimately used for Quantitative Real-Time PCR analysis on LightCycler96 Real-Time PCR system using SYBR Green I Master Mix reagent (Roche). QPCR primers are listed in key resources Table above.

Retroviral Oncogenesis—Retroviral Mouse stem cell virus (MSCV) based plasmid vectors expressing BCR-ABL and NUP98-HOXA9 were transfected into the packaging cell line Platinum-E (a 293T derivative expressing viral structure proteins downstream of the EF1α promoter). Calcium phosphate solution containing HEPES buffered saline (HBS) and Calcium Chloride was used to transfect 30ug of the plasmid DNA into the packaging cells. High titer virus was harvested 48 hours after transfection, filtered, flash frozen and stored in liquid nitrogen. 24 hours before infection, BM cells were harvested from donor mice (Age and sex matched WT and NOX2 KO or FOXC1 f/f; Ai14 mice) and the undifferentiated Lin − cells were sorted by flow cytometry and were cultured overnight in LSK media (IMDM, 10ng/ml IL3, 10ng/ml IL6 and 50ng/ml SCF). The next day 0.75 mL of each virus (BCR-ABL, NUP98-HOXA9) was added to 0.5×10^6 cells re-suspended in 1 mL of 2x LSK media with 16ug polybrene. The infection was repeated 1 more time 8 hours later. Infection efficiency was determined, and equal number of total and leukemic cells were transplanted retroorbitally into unconditioned, syngeneic recipient mice. For secondary transplantation, BCR-ABL and NUP98-HOXA9 double positive leukemic cells were sorted from BM explants of primary recipients and equal numbers of these leukemic cells were injected into secondary recipient mice.

Murine leukemia transplantation—For primary and secondary leukemia transplantation (Figures 2C and 2D) 10,000 leukemic cells were mixed with 100,000 normal carrier BM cells retroorbitally into 8-12 weeks old female C57B/6 recipient mice. 14 days post transplantation, leukemic mice were sacked and spleen as well as BM cells were isolated as described above. For survival analysis, moribund mice were sacked (at variable time points) and the presence of leukemia cells was determined via flow cytometry by harvesting BM and spleen cells. For limit dilution analysis (Figure 2F), The indicated number of LSCs were sorted and mixed with 100,000 normal carrier cells and transplanted retro-orbitally into 8-12 weeks old female C57B/6 recipient mice. 14 days post transplantation, recipient mice were sacked, and the spleen and BM were analyzed for the presence or absence of leukemia via flow cytometry.

shRNA mediated suppression of p22Phox expression—Primary leukemia cells were harvested from the BM of recipients of WT *in vitro* transformed leukemia cells. Leukemic cells were then FACS purified and transduced with a lentiviral vector in a PLKO. 1-Puro backbone expressing an shRNA against CYBA (the gene encoding the p22Phox subunit of the NADPH oxidase complex) for 48 hr. Next, we performed puromycin selection for 72 hours at a dose of 3ug/ml. We cultured cells for an additional 24 hr in fresh media without puromycin. Live cells were sorted, counted and transplanted into secondary

Author Manuscript Author Manuscript Author Manuscript Author Manuscript

recipients at an equal dose of 40,000 cells per mouse. 14 days post transplantation, recipient mice were taken down and disease burden was assessed in the BM and spleen.

Metabolomics—Approximately 4×10^5 leukemia cells were sorted, and metabolomics analyses were performed via ultra-high pressure-liquid chromatography-mass spectrometry (UHPLC-MS – Vanquish and Q Exactive, Thermo Fisher) as previously reported (Nemkov et al. 2017). Briefly, cells were extracted in ice cold methanol:acetonitrile:water (5:3:2 v/v) at a concentration of 1 million cells/ml of buffer. After vortexing for 30 min at 4°C, samples were centrifuged at 15,000 g for 10 min at 4°C and supernatants processed for metabolomics analyses. Ten microliters of sample extracts were loaded onto a Kinetex XB-C18 column (150 × 2.1 mm i.d., 1.7 μm – Phenomenex). A 3 min isocratic run (5% B) and a 9 min gradient from 5%−95% B (phase A: water and B: acetonitrile with + 0.1% formic acid for positive ion mode or with 10 mM ammonium acetate for negative ion mode) were used to elute metabolites. The mass spectrometer scanned in Full MS mode (3 min method) or performed acquisition independent fragmentation (AIF - MS/MS analysis–9 min method) at 70,000 resolution in the 70-900 m/z range, 4 kV spray voltage, 15 sheath gas and 5 auxiliary gas, operated in negative and then positive ion mode (separate runs). Metabolite assignment was performed against an in-house standard library, as reported (Nemkov et al., 2017). Metabolite levels were then normalized to protein quantification.

Seahorse Assays—XF96 (Agilent Technologies, 102417-100) extracellular flux assay kits were used to measure oxygen consumption (OCR) and glycolytic flux (ECAR). Cells were sorted, and directly plated in a XF96 cell culture microplate. OCR and ECAR was measured according to the manufacture protocol and as previously described (Lagadinou et al., 2013). Briefly, five replicate wells of 1×10^5 cells were seeded in a Cell-Tak (Corning, 324240) coated 96-well XF96 well plate. Thirty minutes prior to analysis, the medium was replaced with Seahorse XF media (Agilent Technologies, 102353-100) and the plate was incubated at 37°C. Analyses were performed both at basal conditions and after injection of 5 μg/ml oligomycin (Sigma-Aldrich, 871744), 2 μM FCCP (Sigma-Aldrich, C2920), 5 μM Antimycin A (Sigma-Aldrich, A8774), and 5 μM rotenone (Sigma-Aldrich, R8875).

FAO assay—FAO assay was performed as described previously (Ye et al., 2016). Briefly, sorted Lin− WT and NOX2 KO leukemia cells were cultured in IMDM containing 10 μM palmitate (Sigma) and 10% FBS (Thermo Scientific) overnight and then equal numbers of cells were plated in 48-well plates supplemented with FAO assay medium (IMDM containing 2.5% FBS, 10 μM palmitic acid, 1% fatty acid free BSA (Sigma), 500 μM carnitine (Sigma). Cells were pulsed for 4 hours with 0.5 μCi [9,10-3H(N)]-palmitic acid (Perkinelmer) and the medium was collected to analyze the released 3H2O, formed during cellular oxidation of [3H] palmitate. Briefly, medium was precipitated by 10% trichloroacetic acid (Sigma) and then supernatant was neutralized with 6N NaOH (Sigma) and loaded into ion exchange columns packed with DOWEX 1X2-400 resin (Sigma). The radioactive product was eluted with water and quantitated by liquid scintillation counting.

***In vitro* drug treatment—**Apocynin (sigma-Aldrich) was dissolved in DMSO for a final stock concentration of 10mM. Leukemic cells were cultured *in vitro* and treated with

Author Manuscript Author Manuscript Author Manuscript Author Manuscript

1-100uM doses for 24 hours. The short peptides, Gp91 ds-tat and Scramble ds-tat (Ana-Spec) were dissolved in DMSO at a final stock concentration of 100mM. 0.5 to 50uM doses of each was added into cultured leukemic cells for 3-24 hours.

RNA-Seq: Sample preparation and data analysis—Sca1+Lin− LSCs from the BM of secondary recipients were sorted. A total of 4 mice BM were pooled for each replicate sample used for the analysis. Sort purity was > 98%. Total RNA was extracted using the RNeasy Micro kit (QIAGENE). The total RNA concentration was determined with the NanopDrop 1000 spectrophotometer (NanoDrop) and RNA quality assessed with the Agilent Bioanalyzer (Agilent). The TruSeq Stranded mRNA Sample Preparation Kit (Illumina) was used for next generation sequencing library construction per manufacturer's protocols. Briefly, mRNA was purified from 200ng total RNA with oligo-dT magnetic beads and fragmented. First-strand cDNA synthesis was performed with random hexamer priming followed by second-strand cDNA synthesis using dUTP incorporation for strand marking. End repair and 3′-adenylation was then performed on the double stranded cDNA. Illumina adaptors were ligated to both ends of the cDNA, purified by gel electrophoresis and amplified with PCR primers specific to the adaptor sequences to generate cDNA amplicons of approximately 200-500bp in size. The amplified libraries were hybridized to the Illumina single end flow cell and amplified using the cBot (Illumina). Single end reads of 100nt were generated for each sample using Illumina's HiSeq2500v4. Raw reads generated from Illumina HiSeq2500 sequencing were de-multiplexed using bcl2fastq version 1.8.4. Quality filtering and adaptor removal were performed using Trimmomatic version 0.32 with the following parameters":SLIDINGWINDOW:4:20TRAILING:13LEADING: 13ILLUMINACLIP:adapters.fasta:2:30:10 MINLEN:25." Processed/cleaned reads were then mapped to the reference sequence using the SHRiMP version 2.2.3 alignment software given the following parameters: "–qv-offset 33–all-contigs." Differential expression analyses and data normalization were performed using the CuffDiff tool from the cufflinks version 2.0.2 package given the following parameters: "–FDR 0.05 -u -b GENOME."

GSEA analysis—GSEA analysis was performed using GSEA version 3.0 (Broad institute). FPKM values produced from CuffDiff analysis were formatted into GCT files containing expression values for genes in different biological states. CLS files were manually built to label biological states involved in each study. When performing GSEA analysis, several gene set databases were used including: c2.cp.kegg.v6.0.symbols.gmt, c2.cp.reactome.v6.0.symbols.gmt and an in-house database containing a collection of 860 gene sets of our interest. Following parameters were used: Number of permutations = 1000, permutation type = gene_set, chip platform = annotations_ALL.zip. Other parameters were left at default values.

May-Grunwald Geimsa stain—Cells were cyto-spun onto glass slides at about 0.1e6 concentration per spot at 600RPM for 4 minutes and air-dried for 10 minutes at room temprature. Slides were then stained in May-Grünwald Stain (Sigma) for 5 minutes, followed by a 1.5 minute rinse in Phosphate buffer (sigma). Slides were placed for 20 minutes in Geimsa solution (Sigma) diluted 1:20 with DI water and rinsed for 2 minutes in

Author Manuscript Author Manuscript Author Manuscript Author Manuscript

DI water. After staining, cells were dried at room temperature, mounted in Cytoseal 60 (Thermo Scientific) and submitted for imaging on Zeiss AX10 microscope.

***In vitro* 4OHT and *in vivo* Tamoxifen treatment—**4 Hydroxy-Tamoxifen (Sigma-Aldrich) was dissolved in 100% Ethanol for a stock concentration of 25mM. Cultured leukemic cells were treated with a final concentration of 250nM for 24 hours, washed with FACS buffer and re-plated. For *in vivo* use, Tamoxifen (MP Biomedical) was dissolved in Sunflower oil with 2ul 100% Ethanol per mg of Tamoxifen for a stock concentration of 20mg/ml. 200ul of the stock was injected for a final dose of 4mg into the intra-peritoneal cavity of leukemic mice using a 26-gauge needle.

Protein lysates preparation and WB—Cells were harvested and washed twice in ice cold PBS (0.5% FBS) and resuspended in RIPA lysis and extraction buffer (Thermos Fisher) supplemented with Protease and phosphatase inhibitor cocktail (Thermo fisher) at a concentration of 1xe6 cells per 150 ul. The suspension was incubated on ice for 15 minutes with gentle rocking and centrifuged at 14000 RPM for 15 minutes. 120 ul of clear lysates were transferred to new tubes into which 60 ul of Lammli sample buffer (biorad) was added. Tubes were vortexed briefly and boiled at 95 degrees for 10 minutes. For WB analysis, samples were loaded and resolved on 4 - 15% SDS-PAGE precast gels (biorad), transferred to PVDF membranes, blocked in 5% milk in TBS with 0.1% Triton X-100 (Sigma) for 1 hr. After blocking, the PVDF membranes were rinsed briefly with TBST and incubated with primary antibodies diluted in 5% BSA/TBST at 4°C overnight, washed (5 times 10 minutes each), incubated with secondary antibodies at room temperature for 1 hour at 1:10,000 dilution and washed again and finally subjected to imaging. The WB results were imaged on the ChemiDoc Imaging System (Biorad) and visualized in the Image Lab software (BIO-RAD).

shRNA and lentiviral production—shRNA sequences were constructed into pLKO.1-GFP, which contain a human U6 promoter to drive shRNA expression and a human PGK promoter to drive GFP expression to label shRNA-expressing cells. The detailed methods for generating lentiviral particles, and infecting AML cells are described here (Ashton et al., 2012). Briefly, each pLKO.1-shRNA construct was co-transfected with pPax2 (provides packaging proteins) and pMD2.G (provides VSV-g envelope protein) plasmids into 293T cells (System Bioscience) to produce lentiviral particles. At about 48 hours post transfection, 293T culture supernatants containing lentiviral particles were harvested, filtered, aliquoted and stored in −80°C freezer for future use. At the day of infection, these lentivirus aliquots were thawed and used to infect cells. Primary AML cell were cultured for 3 hours in cytokine supplemented media and were typically infected by mixing 5 e6 cells with 1ml of freshly thawed lentivirus and Polybrene at a final concentration of 8 ug/ml in a 12 well tissue culture plate. At 3-6 days post infection, GFP-positive cells were sorted and analyzed. shRNA targeting sequences are listed in key resources table above.

QUANTIFICATION AND STATISTICAL ANALYSIS

Statistical details for each experiment are indicated in the legend of each figure, where appropriate. The sample size used in each experiment was not predetermined or formally

Author Manuscript Author Manuscript Author Manuscript Author Manuscript

justified for statistical power. In general, for samples with low variation, 3-5 samples per condition were analyzed in each experiment. For samples with larger variation, for instance transplantation experiments, generally 8-12 samples per condition were analyzed in each experiment. Unpaired Student's t test was used to determine significance; P values less than 0.05 were considered significant.

DATA AND SOFTWARE AVAILABILITY

The accession number for the RNA-Seq data reported in this paper is GEO: GSE117657.

Supplementary Material

Refer to Web version on PubMed Central for supplementary material.

ACKNOWLEDGMENTS

We gratefully acknowledge our patients and their families for their participation in this study, Dr. Linda Johnson for help with histopathology analysis, and Drs. Julie Gold, Rachel H. McMahan, and Eric Pietras for providing additional mice used in some studies. We also thank Dr. Patricia Ernst for providing the MSCV-puro plasmid. C.T.J. is supported by the Nancy Carroll Allen Endowed Chair in Hematology and NIH grants R01CA166265 and R01CA200707, and B. A. is supported by Ruth L. Kirschstein Individual Predoctoral National Service Award (F31CA196330-01). C.L.J. is supported by the American Cancer Society (grant 25A5072) and the Colorado Clinical and Translational Sciences Institute (grant AEF CCTSI YR9 CO 2301425). We thank the functional genomics core at University of Colorado Anschutz Medical Campus cancer center(supported in part by grant 5P30CA046934) for providing shRNA constructs.

REFERENCES

Altenhöfer S, Radermacher KA, Kleikers PW, Wingler K, and Schmidt HH (2015). Evolution of NADPH oxidase inhibitors: selectivity and mechanisms for target engagement. Antioxid. Redox Signal 23, 406–427. [PubMed: 24383718]

Ashton JM, Balys M, Neering SJ, Hassane DC, Cowley G, Root DE, Miller PG, Ebert BL, McMurray HR, Land H, and Jordan CT (2012). Gene sets identified with oncogene cooperativity analysis regulate in vivo growth and survival of leukemia stem cells. Cell Stem Cell 11, 359–372. [PubMed: 22863534]

Baillet A, Hograindleur MA, El Benna J, Grichine A, Berthier S, Morel F, and Paclet MH (2017). Unexpected function of the phagocyte NADPH oxidase in supporting hyperglycolysis in stimulated neutrophils: key role of 6-phosphofructo-2-kinase. FASEB J. 31, 663–673. [PubMed: 27799347]

Cabezas-Wallscheid N, Klimmeck D, Hansson J, Lipka DB, Reyes A, Wang Q, Weichenhan D, Lier A, von Paleske L, Renders S, et al. (2014). Identification of regulatory networks in HSCs and their immediate progeny via integrated proteome, transcriptome, and DNA methylome analysis. Cell Stem Cell 15, 507–522. [PubMed: 25158935]

Cancelas JA, Lee AW, Prabhakar R, Stringer KF, Zheng Y, and Williams DA (2005). Rac GTPases differentially integrate signals regulating hematopoietic stem cell localization. Nat. Med 11, 886–891. [PubMed: 16025125]

Chambers SM, Boles NC, Lin KY, Tierney MP, Bowman TV, Bradfute SB, Chen AJ, Merchant AA, Sirin O, Weksberg DC, et al. (2007). Hematopoietic fingerprints: an expression database of stem cells and their progeny. Cell Stem Cell 1, 578–591. [PubMed: 18371395]

Dash AB, Williams IR, Kutok JL, Tomasson MH, Anastasiadou E, Lindahl K, Li S, Van Etten RA, Borrow J, Housman D, et al. (2002). A murine model of CML blast crisis induced by cooperation between BCR/ABL and NUP98/HOXA9. Proc. Natl. Acad. Sci. USA 99, 7622–7627. [PubMed: 12032333]

Dickinson BC, Peltier J, Stone D, Schaffer DV, and Chang CJ (2011). Nox2 redox signaling maintains essential cell populations in the brain. Nat. Chem. Biol 7, 106–112. [PubMed: 21186346]

Author Manuscript Author Manuscript Author Manuscript Author Manuscript

Gal H, Amariglio N, Trakhtenbrot L, Jacob-Hirsh J, Margalit O, Avigdor A, Nagler A, Tavor S, Ein-Dor L, Lapidot T, et al. (2006). Gene expression profiles of AML derived stem cells; similarity to hematopoietic stem cells. Leukemia 20, 2147–2154. [PubMed: 17039238]

Giardino G, Cicalese MP, Delmonte O, Migliavacca M, Palterer B, Loffredo L, Cirillo E, Gallo V, Violi F, and Pignata C (2017). NADPH oxidase deficiency: a multisystem approach. Oxid. Med. Cell. Longev 2017, 4590127. [PubMed: 29430280]

Grauers Wiktorin H, Nilsson T, Aydin E, Hellstrand K, Palmqvist L, and Martner A (2018). Role of NOX2 for leukaemic expansion in a murine model of BCR-ABL1^{+} leukaemia. Br. J. Haematol 182, 290–294. [PubMed: 28542840]

Griffiths HR, Gao D, and Pararasa C (2017). Redox regulation in metabolic programming and inflammation. Redox Biol. 12, 50–57. [PubMed: 28212523]

Groemping Y, and Rittinger K (2005). Activation and assembly of the NADPH oxidase: a structural perspective. Biochem. J 386, 401–416. [PubMed: 15588255]

Han B, Qu Y, Jin Y, Yu Y, Deng N, Wawrowsky K, Zhang X, Li N, Bose S, Wang Q, et al. (2015). FOXC1 activates smoothened-independent Hedgehog signaling in basal-like breast cancer. Cell Rep. 13, 1046–1058. [PubMed: 26565916]

He S, Nakada D, and Morrison SJ (2009). Mechanisms of stem cell self-renewal. Annu. Rev. Cell Dev. Biol 25, 377–406. [PubMed: 19575646]

Ho TC, LaMere M, Stevens BM, Ashton JM, Myers JR, O'Dwyer KM, Liesveld JL, Mendler JH, Guzman M, Morrissette JD, et al. (2016). Evolution of acute myelogenous leukemia stem cell properties after treatment and progression. Blood 128, 1671–1678. [PubMed: 27421961]

Hole PS, Zabkiewicz J, Munje C, Newton Z, Pearn L, White P, Marquez N, Hills RK, Burnett AK, Tonks A, and Darley RL (2013). Overproduction of NOX-derived ROS in AML promotes proliferation and is associated with defective oxidative stress signaling. Blood 122, 3322–3330. [PubMed: 24089327]

Ito K, Hirao A, Arai F, Takubo K, Matsuoka S, Miyamoto K, Ohmura M, Naka K, Hosokawa K, Ikeda Y, and Suda T (2006). Reactive oxygen species act through p38 MAPK to limit the lifespan of hematopoietic stem cells. Nat. Med 12, 446–451. [PubMed: 16565722]

Jiang F, Zhang Y, and Dusting GJ (2011). NADPH oxidase-mediated redox signaling: roles in cellular stress response, stress tolerance, and tissue repair. Pharmacol. Rev 63, 218–242. [PubMed: 21228261]

Juntilla MM, Patil VD, Calamito M, Joshi RP, Birnbaum MJ, and Koretzky GA (2010). AKT1 and AKT2 maintain hematopoietic stem cell function by regulating reactive oxygen species. Blood 115, 4030–4038. [PubMed: 20354168]

Kumar MS, Pester RE, Chen CY, Lane K, Chin C, Lu J, Kirsch DG, Golub TR, and Jacks T (2009). Dicer1 functions as a haploinsufficient tumor suppressor. Genes Dev. 23, 2700–2704. [PubMed: 19903759]

Lagadinou ED, Sach A, Callahan K, Rossi RM, Neering SJ, Minhajuddin M, Ashton JM, Pei S, Grose V, O'Dwyer KM, et al. (2013). BCL-2 inhibition targets oxidative phosphorylation and selectively eradicates quiescent human leukemia stem cells. Cell Stem Cell 12, 329–341. [PubMed: 23333149]

Lay K, Kume T, and Fuchs E (2016). FOXC1 maintains the hair follicle stem cell niche and governs stem cell quiescence to preserve long-term tissue-regenerating potential. Proc. Natl. Acad. Sci. USA 113, E1506–E1515. [PubMed: 26912458]

Le Belle JE, Orozco NM, Paucar AA, Saxe JP, Mottahedeh J, Pyle AD, Wu H, and Kornblum HI (2011). Proliferative neural stem cells have high endogenous ROS levels that regulate self-renewal and neurogenesis in a PI3K/Akt-dependant manner. Cell Stem Cell 8, 59–71. [PubMed: 21211782]

Lunt SY, and Vander Heiden MG (2011). Aerobic glycolysis: meeting the metabolic requirements of cell proliferation. Annu. Rev. Cell Dev. Biol 27, 441–464. [PubMed: 21985671]

Marlein CR, Zaitseva L, Piddock RE, Robinson SD, Edwards DR, Shafat MS, Zhou Z, Lawes M, Bowles KM, and Rushworth SA (2017). NADPH oxidase-2 derived superoxide drives mitochondrial transfer from bone marrow stromal cells to leukemic blasts. Blood 130, 1649–1660. [PubMed: 28733324]

Author Manuscript Author Manuscript Author Manuscript Author Manuscript

Moloney JN, Stanicka J, and Cotter TG (2017). Subcellular localization of the FLT3-ITD oncogene plays a significant role in the production of NOX- and $p22^{phox}$-derived reactive oxygen species in acute myeloid leukemia. Leuk. Res 52, 34–42. [PubMed: 27870947]

Moran-Crusio K, Reavie L, Shih A, Abdel-Wahab O, Ndiaye-Lobry D, Lobry C, Figueroa ME, Vasanthakumar A, Patel J, Zhao X, et al. (2011). Tet2 loss leads to increased hematopoietic stem cell self-renewal and myeloid transformation. Cancer Cell 20, 11–24. [PubMed: 21723200]

Morimoto H, Iwata K, Ogonuki N, Inoue K, Atsuo O, Kanatsu-Shinohara M, Morimoto T, Yabe-Nishimura C, and Shinohara T (2013). ROS are required for mouse spermatogonial stem cell self-renewal. Cell Stem Cell 12, 774–786. [PubMed: 23746981]

Myant KB, Cammareri P, McGhee EJ, Ridgway RA, Huels DJ, Cordero JB, Schwitalla S, Kalna G, Ogg EL, Athineos D, et al. (2013). ROS production and NF-κB activation triggered by RAC1 facilitate WNT-driven intestinal stem cell proliferation and colorectal cancer initiation. Cell Stem Cell 12, 761–773. [PubMed: 23665120]

Neering SJ, Bushnell T, Sozer S, Ashton J, Rossi RM, Wang PY, Bell DR, Heinrich D, Bottaro A, and Jordan CT (2007). Leukemia stem cells in a genetically defined murine model of blast-crisis CML. Blood 110, 2578–2585. [PubMed: 17601986]

Nemkov T, Hansen KC, and D'Alessandro A (2017). A three-minute method for high-throughput quantitative metabolomics and quantitative tracing experiments of central carbon and nitrogen pathways. Rapid Commun. Mass Spectrom 31, 663–673. [PubMed: 28195377]

Omatsu Y, Seike M, Sugiyama T, Kume T, and Nagasawa T (2014). Foxc1 is a critical regulator of haematopoietic stem/progenitor cell niche formation. Nature 508, 536–540. [PubMed: 24590069]

Owusu-Ansah E, and Banerjee U (2009). Reactive oxygen species prime Drosophila haematopoietic progenitors for differentiation. Nature 461, 537–541. [PubMed: 19727075]

Panday A, Sahoo MK, Osorio D, and Batra S (2015). NADPH oxidases: an overview from structure to innate immunity-associated pathologies. Cell. Mol. Immunol 12, 5–23. [PubMed: 25263488]

Pietras EM, Reynaud D, Kang YA, Carlin D, Calero-Nieto FJ, Leavitt AD, Stuart JM, Göttgens B, and Passegué E (2015). Functionally distinct subsets of lineage-biased multipotent progenitors control blood production in normal and regenerative conditions. Cell Stem Cell 17, 35–46. [PubMed: 26095048]

Pollock JD, Williams DA, Gifford MA, Li LL, Du X, Fisherman J, Orkin SH, Doerschuk CM, and Dinauer MC (1995). Mouse model of X-linked chronic granulomatous disease, an inherited defect in phagocyte superoxide production. Nat. Genet 9, 202–209. [PubMed: 7719350]

Reddy MM, Fernandes MS, Salgia R, Levine RL, Griffin JD, and Sattler M (2011). NADPH oxidases regulate cell growth and migration in myeloid cells transformed by oncogenic tyrosine kinases. Leukemia 25, 281–289. [PubMed: 21072051]

Roberts AW, Kim C, Zhen L, Lowe JB, Kapur R, Petryniak B, Spaetti A, Pollock JD, Borneo JB, Bradford GB, et al. (1999). Deficiency of the hematopoietic cell-specific Rho family GTPase Rac2 is characterized by abnormalities in neutrophil function and host defense. Immunity 10, 183–196. [PubMed: 10072071]

Sasman A, Nassano-Miller C, Shim KS, Koo HY, Liu T, Schultz KM, Millay M, Nanano A, Kang M, Suzuki T, and Kume T (2012). Generation of conditional alleles for Foxc1 and Foxc2 in mice. Genesis 50, 766–774. [PubMed: 22522965]

Seita J, and Weissman IL (2010). Hematopoietic stem cell: self-renewal versus differentiation. Wiley Interdiscip. Rev. Syst. Biol. Med 2, 640–653. [PubMed: 20890962]

Sengupta A, Arnett J, Dunn S, Williams DA, and Cancelas JA (2010). Rac2 GTPase deficiency depletes BCR-ABL+ leukemic stem cells and progenitors in vivo. Blood 116, 81–84. [PubMed: 20407032]

Shao L, Li H, Pazhanisamy SK, Meng A, Wang Y, and Zhou D (2011). Reactive oxygen species and hematopoietic stem cell senescence. Int. J. Hematol 94, 24–32. [PubMed: 21567162]

Shima Y, Yumoto M, Katsumoto T, and Kitabayashi I (2017). MLL is essential for NUP98-HOXA9-induced leukemia. Leukemia 31, 2200–2210. [PubMed: 28210005]

Somerville TD, Wiseman DH, Spencer GJ, Huang X, Lynch JT, Leong HS, Williams EL, Cheesman E, and Somervaille TC (2015). Frequent derepression of the mesenchymal transcription factor gene FOXC1 in acute myeloid leukemia. Cancer Cell 28, 329–342. [PubMed: 26373280]

Author Manuscript Author Manuscript Author Manuscript Author Manuscript

Subramanian A, Tamayo P, Mootha VK, Mukherjee S, Ebert BL, Gillette MA, Paulovich A, Pomeroy SL, Golub TR, Lander ES, and Mesirov JP (2005). Gene set enrichment analysis: a knowledge-based approach for interpreting genome-wide expression profiles. Proc. Natl. Acad. Sci. USA 102, 15545–15550. [PubMed: 16199517]

Takizawa H, Fritsch K, Kovtonyuk LV, Saito Y, Yakkala C, Jacobs K, and Manz MG (2017). Pathogen-induced TLR4-TRIF innate immune signaling in hematopoietic stem cells promotes proliferation but reduces competitive fitness. Cell Stem Cell 21, 225–240.e225. [PubMed: 28736216]

Tothova Z, Kollipara R, Huntly BJ, Lee BH, Castrillon DH, Cullen DE, McDowell EP, Lazo-Kallanian S, Williams IR, Sears C, et al. (2007). FoxOs are critical mediators of hematopoietic stem cell resistance to physiologic oxidative stress. Cell 128, 325–339. [PubMed: 17254970]

Wang L, Siegenthaler JA, Dowell RD, and Yi R (2016). Foxc1 reinforces quiescence in self-renewing hair follicle stem cells. Science 351, 613–617. [PubMed: 26912704]

Weisser M, Demel UM, Stein S, Chen-Wichmann L, Touzot F, Santilli G, and Grez M (2016). Hyperinflammation in patients with chronic granulomatous disease leads to impairment of hematopoietic stem cell functions. J. Allergy Clin. Immunol 138, 219–228.e219. [PubMed: 26853280]

Wilm B, James RG, Schultheiss TM, and Hogan BL (2004). The forkhead genes, Foxc1 and Foxc2, regulate paraxial versus intermediate mesoderm cell fate. Dev. Biol 271, 176–189. [PubMed: 15196959]

Wilson A, Laurenti E, Oser G, van der Wath RC, Blanco-Bose W, Jaworski M, Offner S, Dunant CF, Eshkind L, Bockamp E, et al. (2008). Hematopoietic stem cells reversibly switch from dormancy to self-renewal during homeostasis and repair. Cell 135, 1118–1129. [PubMed: 19062086]

Yang L, Wang L, Geiger H, Cancelas JA, Mo J, and Zheng Y (2007). Rho GTPase Cdc42 coordinates hematopoietic stem cell quiescence and niche interaction in the bone marrow. Proc. Natl. Acad. Sci. USA 104, 5091–5096. [PubMed: 17360364]

Ye H, Adane B, Khan N, Sullivan T, Minhajuddin M, Gasparetto M, Stevens B, Pei S, Balys M, Ashton JM, et al. (2016). Leukemic stem cells evade chemotherapy by metabolic adaptation to an adipose tissue niche. Cell Stem Cell 19, 23–37. [PubMed: 27374788]

Author Manuscript Author Manuscript Author Manuscript Author Manuscript

Highlights

- Depletion of NOX2 reduces basal ROS levels and impairs core metabolism
- NOX2 regulates self-renewal- and differentiation-associated transcriptional programs
- Downstream of NOX2, FOXC1 controls part of the differentiation program
- Depletion of FOXC1 or NOX2 impairs leukemogenesis in murine models and xenografts

Author Manuscript Author Manuscript Author Manuscript Author Manuscript

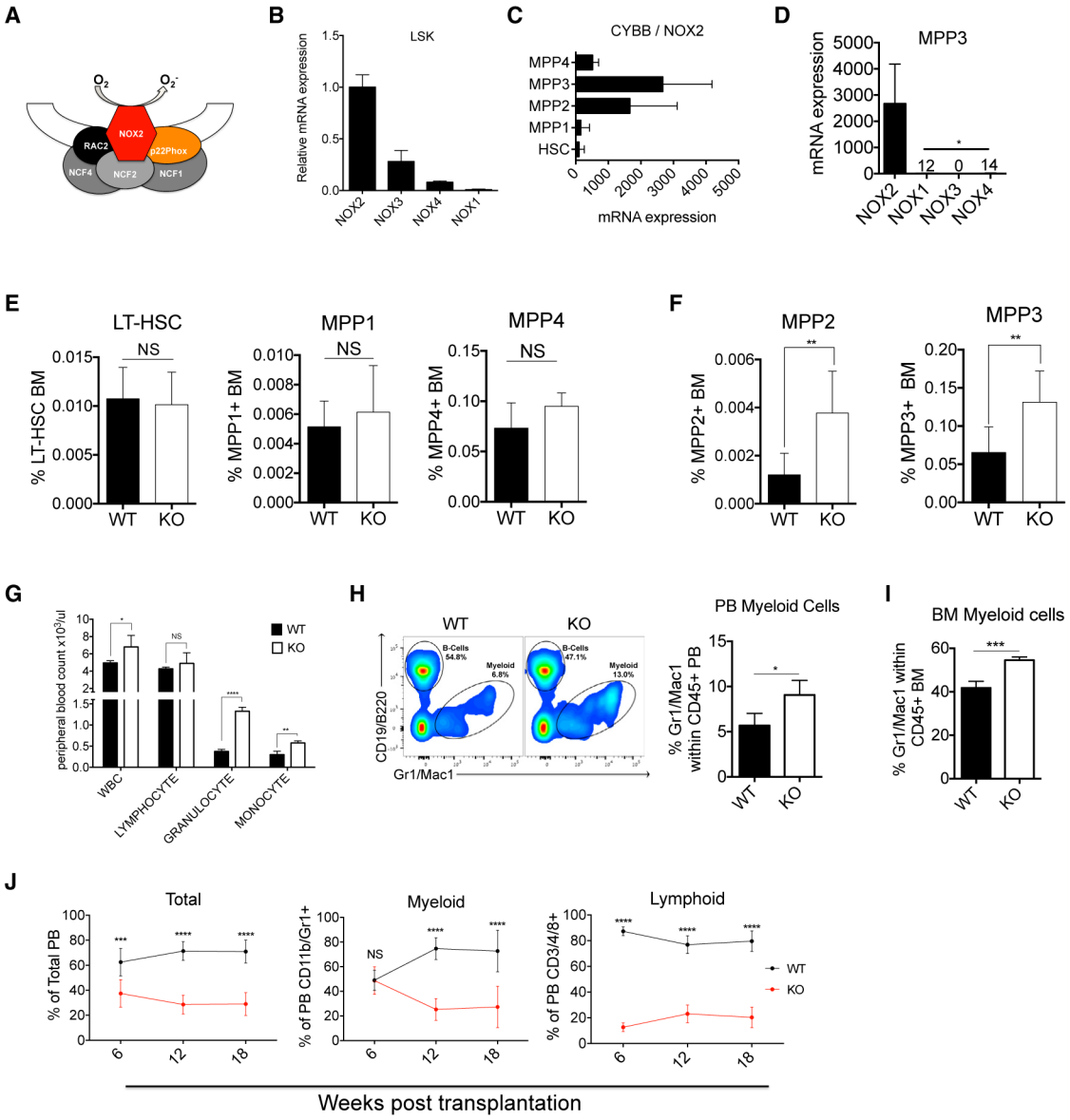

Figure 1. NOX2 Is Expressed in HSPCs, and Its Deficiency Compromises Steady-State and Regenerative Hematopoiesis

(A) Schematics showing the subunits making up the canonical NADPH oxidase 2 complex.

(B) mRNA expression of all 4 murine paralogs of NADPH oxidase genes in purified LSK cells.

(C) mRNA expression levels of NOX2 in primitive hematopoietic cells. Data are mined from previously reported RNA-seq results (Cabezas-Wallscheid et al., 2014)

(D) mRNA expression of all 4 murine paralogs of NADPH oxidase genes in MPP3 cells.

(E) Frequency of LT-HSCs, MPP1, and MPP4 cells in total live BM from age- and sex-matched WT and NOX2 KO mice. n = 8, two independent experiments.

(F) Frequency of MPP2 and MPP3 cells in total live BM from age- and sex-matched WT and NOX2 KO mice. n = 8, two independent experiments.

Author Manuscript Author Manuscript Author Manuscript Author Manuscript

(G) Differential cell count on the peripheral blood (PB) of age- and sex-matched WT and NOX2 KO mice. n = 5, representative of 3 independent experiments.
(H) Representative flow cytometric plot showing the composition of PB (left) and the frequency of Gr1/CD11b$^+$ myeloid cells in total CD45$^+$ live BM from age- and sex-matched WT and NOX2 KO mice (right). n = 5.
(I) Frequency of Gr1/CD11b$^+$ myeloid cells in total CD45$^+$ live BM from age- and sex-matched WT and NOX2 KO mice. n = 5.
(J) Competitive transplantation of 500,000 whole BM cells from WT and NOX2 KO mice into irradiated WT recipients. The contribution of donor and competitor cells in PB is shown.
Bars represent mean ± SD. *$p < 0.05$; **$p < 0.01$; ***$p < 0.001$; ****$p < 0.0001$; ns, not significant, unpaired Student's t test.

Author Manuscript Author Manuscript Author Manuscript Author Manuscript

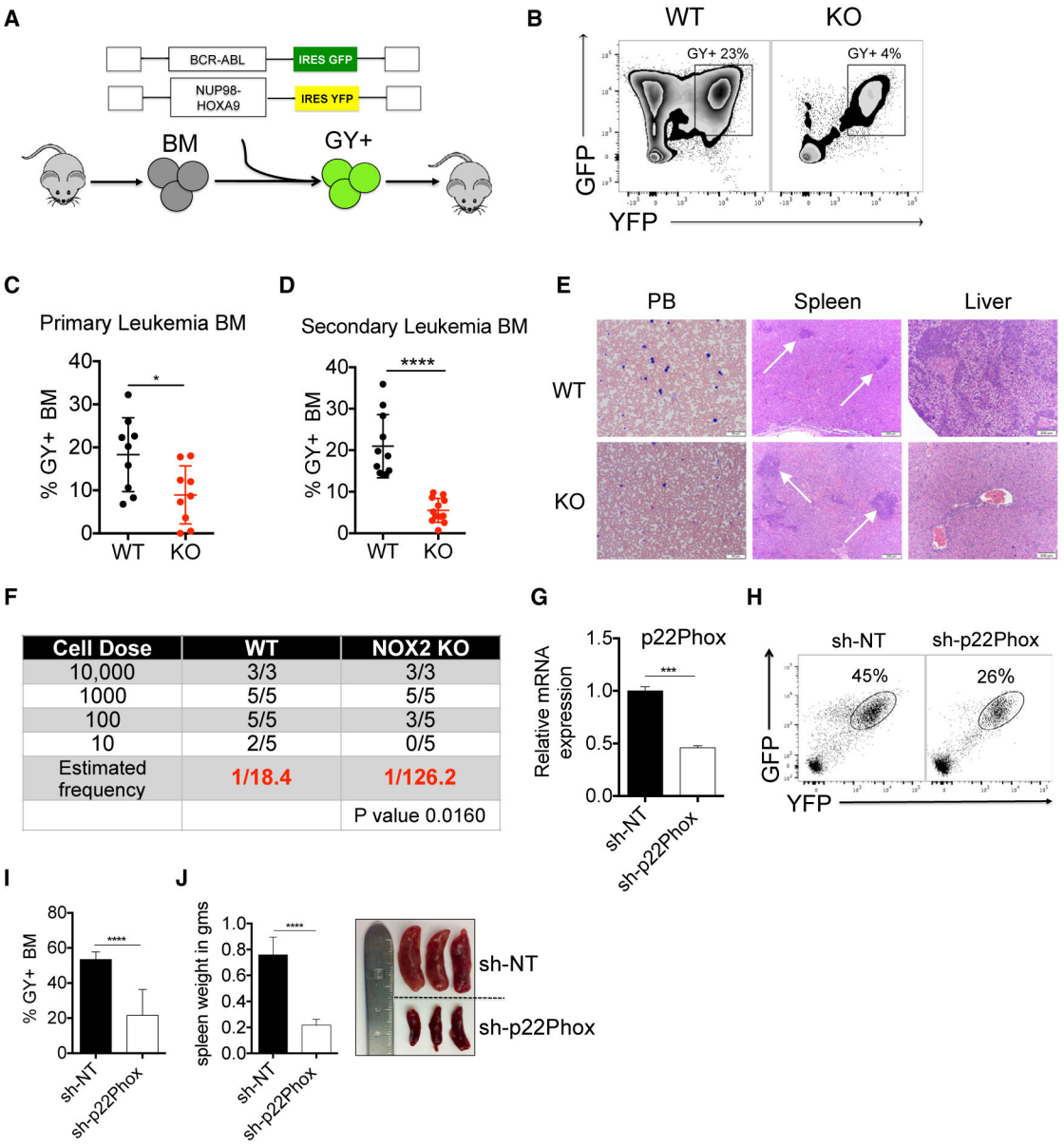

Cell Dose	WT	NOX2 KO
10,000	3/3	3/3
1000	5/5	5/5
100	5/5	3/5
10	2/5	0/5
Estimated frequency	1/18.4	1/126.2
		P value 0.0160

Figure 2. Deficiency of the NOX2 Complex Attenuates Leukemogenesis *In Vivo*

(A) Schematics showing retroviral oncogenesis model used to generate murine leukemia.

(B) Representative flow cytometric plot showing frequency of leukemic cells in the BM of recipients of primary WT and NOX2 KO leukemia.

(C) Frequency of leukemic cells in the BM of primary recipients of leukemic cells. n = 9.

(D) Frequency of leukemic cells in the BM of secondary recipients. WT, n = 11; KO, n = 12.

(E) Cytospin preparation of PB (left) and H&E staining of sections of spleen (middle) and liver (right) from secondary recipients of WT and NOX2 KO leukemia. Arrows show splenic nodules that are relatively better preserved in KO leukemias. Additional supporting data are presented in Figures S2E and S2F. Scale bars represent 50 μm for PB and 200 μm for spleen and liver.

Author Manuscript Author Manuscript Author Manuscript Author Manuscript

(F) Limiting dilution analysis showing the frequency of leukemia-initiating stem cell populations from secondary WT or NOX2 KO leukemic cells.
(G) shRNA-mediated suppression of mRNA expression of the p22Phox subunit of NOX2.
(H) Representative flow cytometric plot showing BM disease burden of leukemic cells in recipients of non-targeting shRNA (shNT) and shp22Phox leukemic cells.
(I) Frequency of leukemic cells in the BM of recipients of shNT and shp22Phox leukemic cells. n = 10.
(J) The weight of spleen extracted from recipients of shNT or shp22Phox leukemia cells (left) and representative images (right).
Bars represent mean ± SD. *$p < 0.05$; **$p < 0.01$; ***$p < 0.001$; ****$p < 0.0001$; ns, not significant, unpaired Student's t test.

Author Manuscript Author Manuscript Author Manuscript Author Manuscript

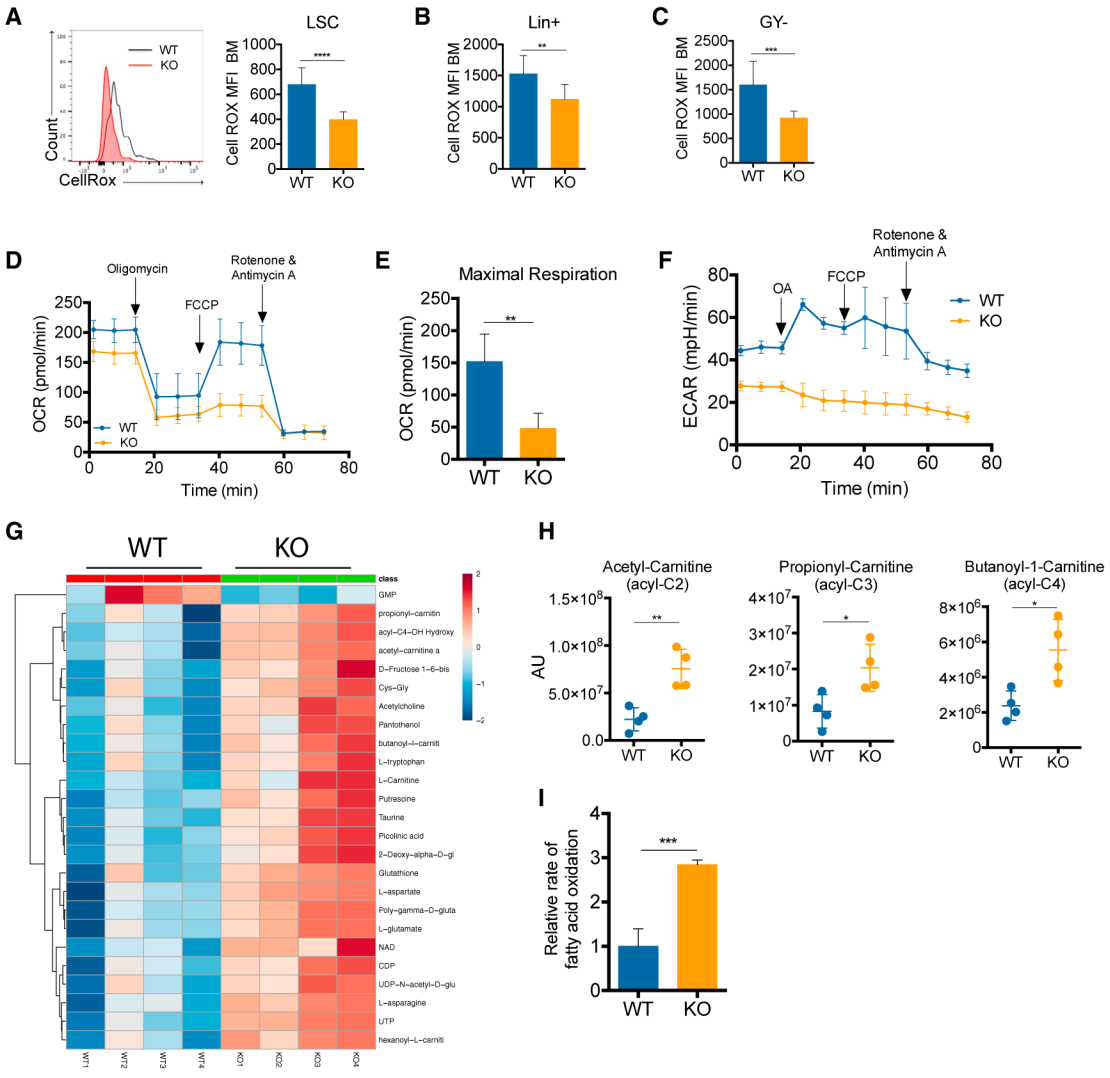

Figure 3. Suppression of NOX2 Reduces Basal ROS and Impairs Core Metabolism

(A) Representative histogram showing the fluorescence of CellROX within the leukemia-initiating stem cell population (LSC) compartment of leukemic cells (left) and mean fluorescence intensity of CellROX (right). n = 10.

(B) Mean fluorescence intensity of CellROX in the lineage-positive compartment of leukemic cells. n = 10.

(C) Mean fluorescence intensity of CellROX of the GFP/YFP− (GY−) non-leukemic cells co-inhabiting the bone marrow with eitherWT or NOX2 KO leukemia. n = 10.

(D) Relative rate of oxygen consumption in WT and NOX2 KO secondary leukemia cells.

(E) Maximal respiration rate of WT and NOX2 KO leukemia cells.

(F) Extracellular acidification rates (proxy for glycolytic potential) of WT and NOX2 KO leukemic cells.

(D–F) n = 5 technical replicates, representative of 2 independent experiments.

(G) Heatmap showing the relative abundance of the most significantly altered metabolites detected in WT and NOX2 KO leukemia cells via mass spectrometry. n = 4 technical replicates.

Author Manuscript Author Manuscript Author Manuscript Author Manuscript

(H) The relative abundance of carnitine-conjugated short-chain free fatty acids from WT and NOX2 KO leukemia cells.

(I) The relative rate of tritium-labeled palmitic acid oxidation in WT and NOX2 KO leukemia cells as measured by quantitating the cleavage of radioactive hydrogen via scintillation counts. n = 4 technical replicates.

Bars represent mean ± SD. *p < 0.05; **p < 0.01; ***p < 0.001; ****p < 0.0001; ns, not significant, unpaired Student's t test.

Author Manuscript Author Manuscript Author Manuscript Author Manuscript

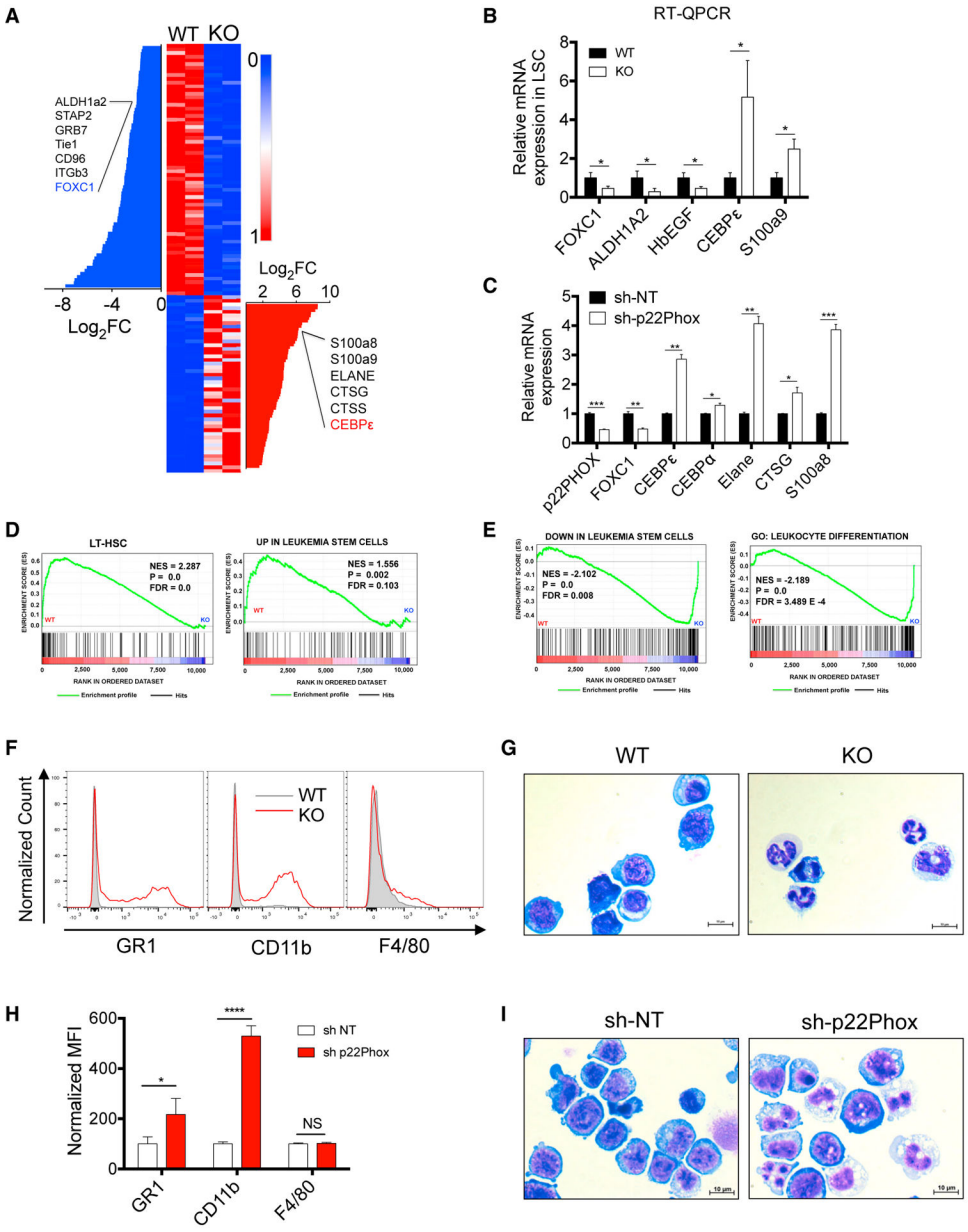

Figure 4. NOX2 KO LSCs Lose a Stem Cell-Associated Transcriptional Program and Undergo Terminal Differentiation

(A) Heatmap shows normalized fragments per kilobase of transcript per million mapped reads (FPKM) values of the most significantly dysregulated genes in WT and NOX2 KO LSCs. Log2 values of the fold change for the selected up- and downregulated genes are shown as waterfall bar graphs.

(B) The expression level of the indicated genes is measured by qRT-PCR as a validation of the RNA-seq result in an independent cohort of LSCs. Bars represent mean ± SD. *p < 0.05; unpaired Student's t test.

(C) LSCs were sorted from the bone marrow of recipients of shNT and shp22Phox leukemia; n = 10. The relative expression level of several genes was determined by qRT-QPCR.

Author Manuscript Author Manuscript Author Manuscript Author Manuscript

(D) GSEA showing enrichment of LT-HSC program (left) and leukemia stem cell upregulated genes (right) in WT LSCs relative to NOX2 KO LSCs. NES, p value and false discovery rate (FDR) according Subramanian et al. (2005).
(E) GSEA showing enrichment of differentiation program (right) and leukemia stem cell downregulated genes (left) in NOX2 KO LSCs relative to WT LSCs.
(F) Representative histogram plot showing the relative expression levels of the myeloid surface antigens Gr1, CD11b, and F4/80 in BM explants of WT and NOX2 KO leukemia.
(G) Images showing the morphology of WT and NOX2 KO leukemia cells analyzed via May-Grünwald-Giemsa staining. Additional images are shown in Figure S4F. Scale bars represent 10 μm.
(H) Relative expression of the myeloid-differentiation-associated surface antigens Gr1, CD11b, and F4/80 in control and shp22Phox leukemia cells harvested from BM.
(I) Images showing the morphology of control and p22Phox KD leukemia cells analyzed via May-Grünwald-Giemsa staining. Additional images are shown in Figure S4G.

Author Manuscript Author Manuscript Author Manuscript Author Manuscript

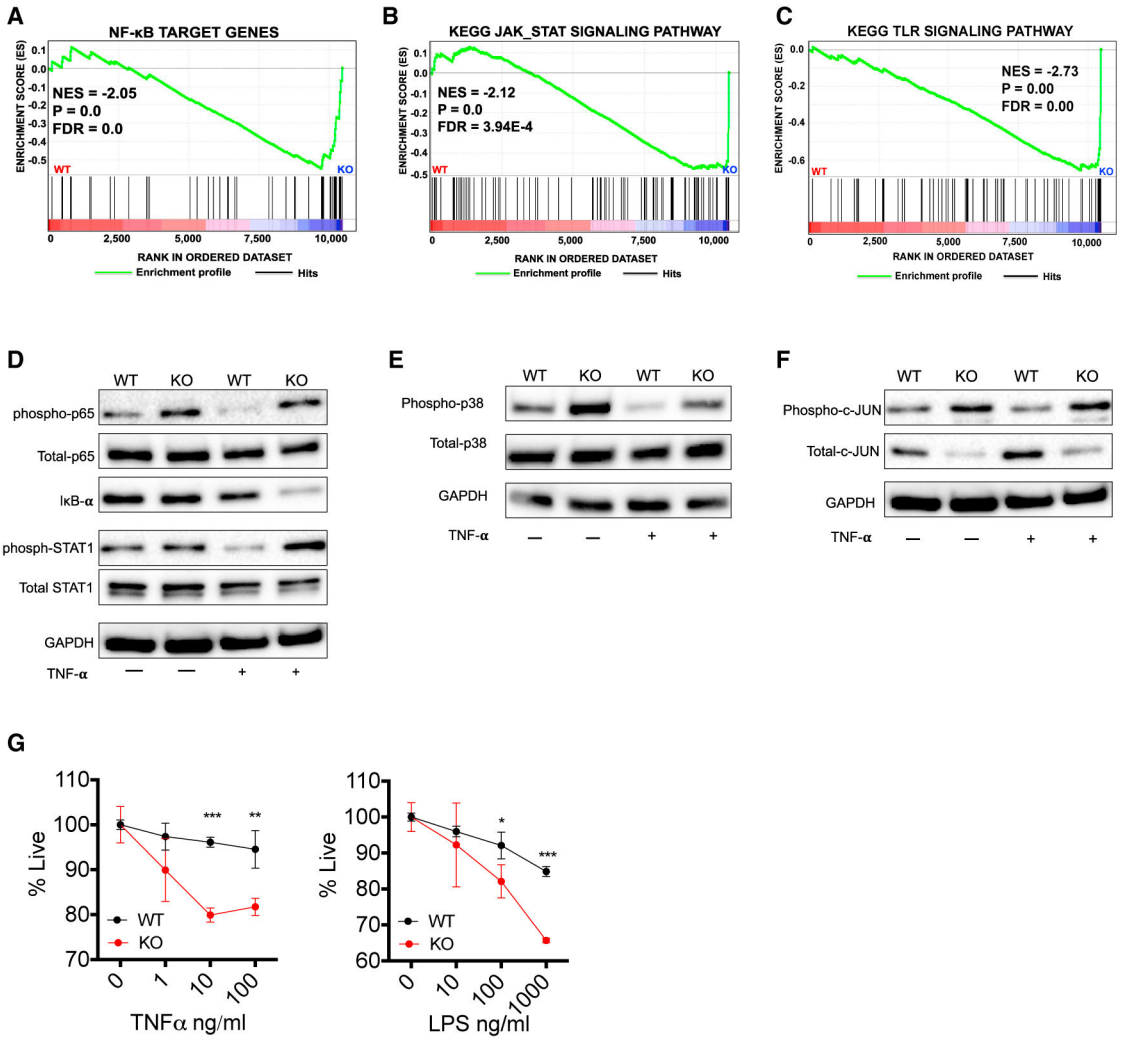

Figure 5. NOX2 Regulates Inflammatory Signaling in Leukemic Cells

(A) GSEA showing the enrichment of NF-κB target genes in NOX2 KO LSCs.

(B) GSEA showing the enrichment of components of the JAK-STAT signaling pathway in NOX2 KO LSCs.

(C) GSEA showing the enrichment of components of the Toll-like receptor (TLR) signaling pathway in NOX2 KO LSCs.

(A–C) NES represents the p value and FDR according to Subramanian et al. (2005).

(D) Immunoblot analysis of total and phospho p65(S536), Ikbα3, and total and phospho STAT1(S727) in WT and NOX2 KO leukemia cells treated with control or 10 ng/mL TNF-α for 30 min. GAPDH was used as a loading control.

(E) Immunoblot analysis of total and phospho p38 MAPK (Thr180/Tyr182) in WT and NOX2 KO leukemia cells treated with control or 10 ng/mL TNF-α for 30 min. GAPDH was used as a loading control.

(F) Immunoblot analysis of total and phospho c-Jun (S73) in WT and NOX2 KO leukemia cells treated with control or 10 ng/mL TNF-α for 30 min. GAPDH was used as a loading control.

(G) WT or NOX2 KO cells were cultured *in vitro* in the presence of increasing doses of TNF-α (left) or lipopolysaccharides (LPSs; right). Cell viability was measured 72 h later with Annexin V, DAPI staining.

Author Manuscript Author Manuscript Author Manuscript Author Manuscript

Author Manuscript Author Manuscript Author Manuscript Author Manuscript

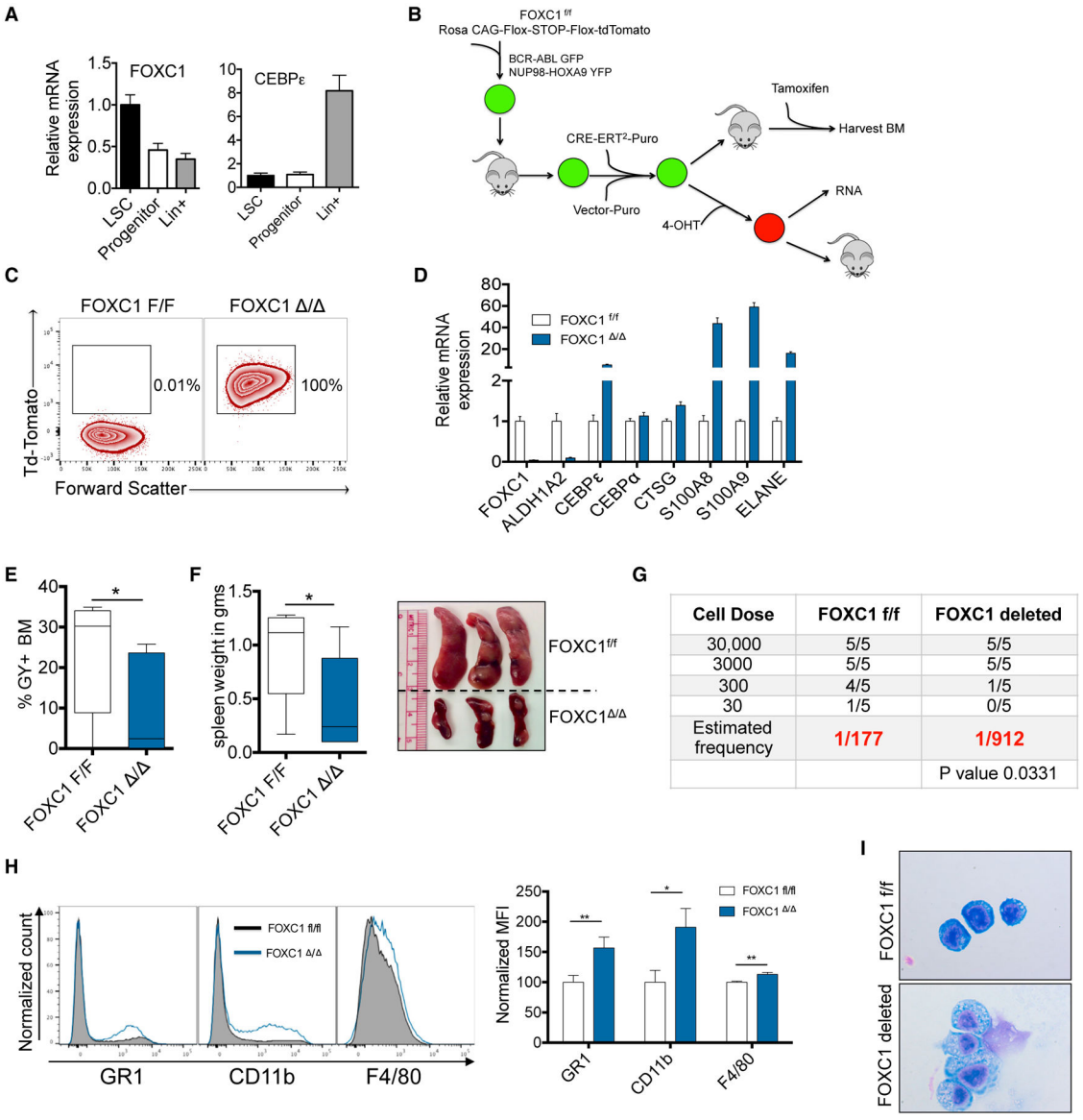

Cell Dose	FOXC1 f/f	FOXC1 deleted
30,000	5/5	5/5
3000	5/5	5/5
300	4/5	1/5
30	1/5	0/5
Estimated frequency	1/177	1/912
		P value 0.0331

Figure 6. FOXC1 Regulates Leukemogenesis Downstream of NOX2

(A) Relative mRNA expression level of *FOXC1* and *CEBPε* in the different subpopulations of leukemic cells is shown. LSCs (Sca1+Lin−), progenitor (Sea1−Lin−).

(B) Schematic showing the experimental strategy utilized to study the role of FOXC1.

(C) Flow cytometric plot showing efficient activation of the CRE recombinase activity reporter td-Tomato in 4-OHT-treated CRE-ERT2-expressing leukemic cells relative to controls.

(D) qRT-PCR based measurement of mRNA expression ofthe indicated genes in *FOXC1* deleted leukemic cells.

(E) The frequency of leukemia cells in the BM of recipients of control or FOXC1-deleted leukemia cells is shown as whiskers minimum-to-maximum plot; the line inside the box represents the mean, and the top and bottom lines represent the 75% and 25% percentiles. The lines above and below represent SD. n = 10. *p < 0.05, unpaired Student's t test.

Author Manuscript Author Manuscript Author Manuscript Author Manuscript

(F) Weight of spleens (left) and a representative picture of spleens (right) harvested from leukemic mice are shown.
(G) Limiting dilution analysis of control and FOXC1-deleted leukemia cells.
(H) Representative histogram (left) and mean fluorescence intensity of the relative expression levels of the myeloid surface antigens Gr1, CD11b, and F4/80 in BM explants of control and FOXC1-deleted leukemia.
(I) Images showing the morphology of control and FOXC1-deleted leukemia cells analyzed via May-Grünwald-Giemsa staining. Additional images are shown in Figure S6H.

Author Manuscript Author Manuscript Author Manuscript Author Manuscript

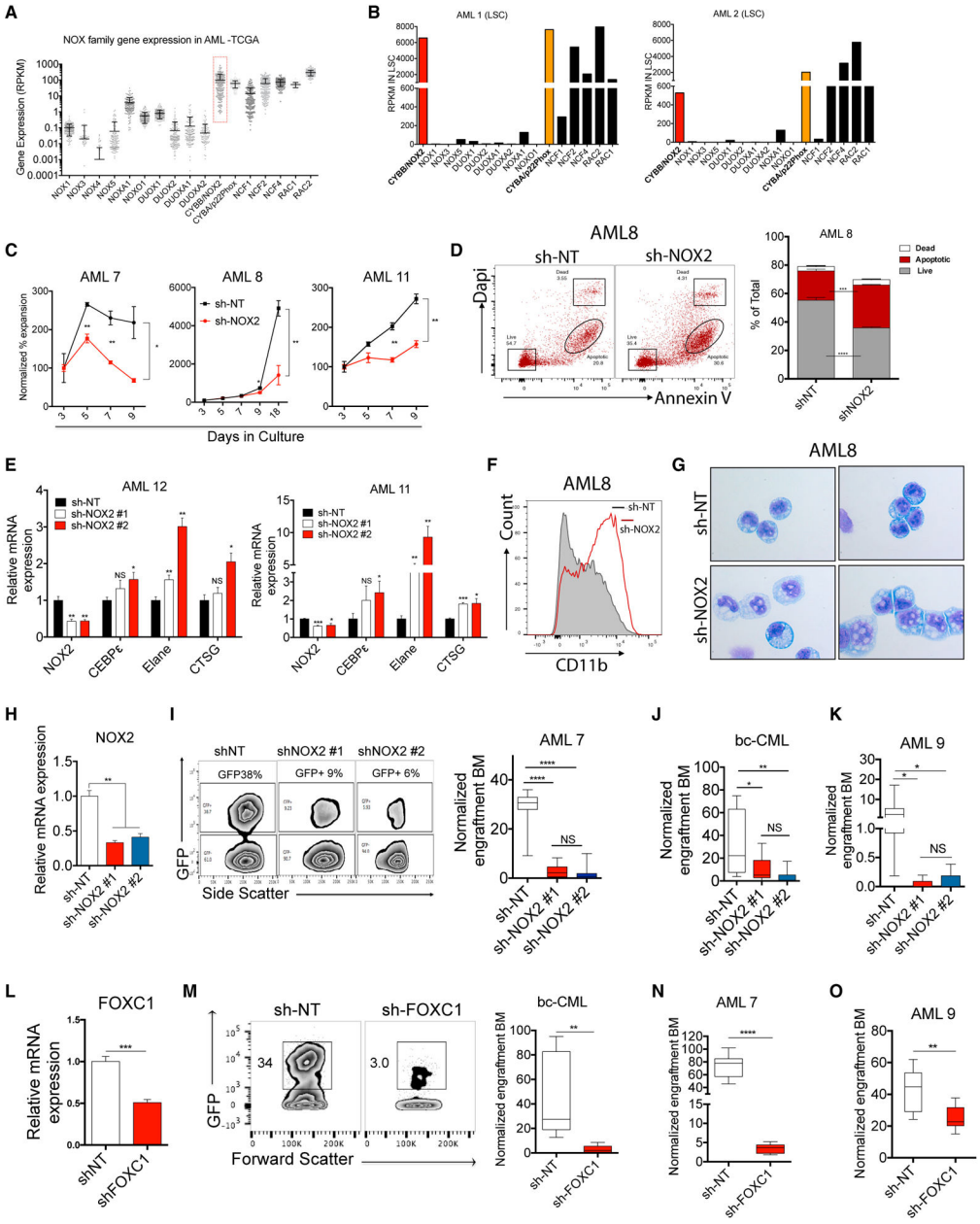

Figure 7. NOX2 and FOXC1 Are Important for the Growth of Primary Human Myeloid Leukemia Cells

(A) The Cancer Genome Atlas (TCGA) database for AML was used to analyze the expression levels of several NADPH-dependent oxidases (NOX1–NOX5), accessory subunits (NCF1, NCF2, NCF4, NOXA1, NOXO1, p22Phox, RAC1, and RAC2) as well as related oxido-reductase enzymes (dual-oxidases 1,2, A2). The reads per kilobase of transcript per million mapped reads (RPKM) values for each gene in a total of 188 AMLs are shown.

(B) RNA-seq analysis was performed on functionally validated leukemic stem cells isolated from human primary AMLs. The RPKM value for each gene is shown. Unpublished data are used with permission. Additional supporting data are shown in Figure S7A.

Author Manuscript Author Manuscript Author Manuscript Author Manuscript

(C) Equal numbers of control or shNOX2-transduced primary AML cells were cultured *in vitro* in the presence of 10 ng/mL of IL-3, SCF, and FL3, and the relative percent expansion is reported for each specimen. n = 3, mean ± SD. *p < 0.05; **p < 0.01.
(D) Control and shNOX2 primary AML cells were purified and cultured *in vitro* for 12 days. Annexin V, DAPI staining was performed to evaluate the degree of apoptotic cell death. A representative flow plot (left) and quantitation of 3 technical triplicates (right) are shown. Additional data are shown in Figure S7B.
(E) The relative expression level of *NOX2*, *CEBPε*, *Elane*, and *CTSG* is shown in AML specimens in which NOX2 was knocked down using shRNAs. Additional supporting data are provided in Figure S7D.
(F) Histogram showing the relative expression of the myeloid surface antigen CD11b in control and NOX2 KD primary human AML cells cultured *in vitro*.
(G) Images showing the morphology of control and NOX2 KD primary AML cells analyzed via May-Grünwald-Giemsa staining.
(H) Relative level of expression of NOX2 is shown in control and shNOX2 primary AML cells used in xenograft analysis.
(I) Representative flow cytometric plot showing the level of GFP+ (human leukemic cells bearing control or shNOX2) leukemic cells explanted from the BM of recipient mice (left), and quantitation of the relative normalized engraftment, defined as(% $CD45^+$GFP+ BM at harvest/% $CD45^+$ GFP+ BM pre-transplant) × 100 (right). Data are shown as whiskers minimum-to-maximum plot; the line inside the box represents the mean, and the top and bottom lines represent the 75% and 25% percentiles. The lines above and below represent SD. n = 9. ****p < 0.0001, unpaired Student's t test.
(J) Relative engraftment levels of a bc-CML specimen in which NOX2 is knocked down.
(K) Relative engraftment levels of an AML specimen in which NOX2 is knocked down.
(L) The relative level of expression of FOXC1 is shown in control and shFOXC1 primary bc-CML specimen used in xenograft analysis.
(M) Similar analysis as in (I) but performed for FOXC1 knockdown xenografts of the bc-CML specimen.
(N) Relative engraftment levels of control and FOXC1 KD groups in an AML specimen expressing high levels of FOXC1.
(O) Relative engraftment levels of control and FOXC1 KD groups in an additional AML specimen expressing high levels of FOXC1.

Author Manuscript Author Manuscript Author Manuscript Author Manuscript

KEY RESOURCES TABLE

REAGENT or RESOURCE	SOURCE	IDENTIFIER
Antibodies		
CD45R APC-CY7	BD Biosciences	552094
TER119 APC-CY7	BD Biosciences	560509
Gr1 APC-CY7	BD Biosciences	557661
CD11b APC-CY7	BD Biosciences	557657
CD3 APC-CY7	Biolegend	100222
CD19 APC	eBiosciences	17-0191-82
CD45R APC	eBiosciences	17-0452-82
CD3e PE-CY7	BD Biosciences	552774
CD4 PE-CY7	BD Biosciences	552775
CD8a PE-CY7	BD Biosciences	552877
CD45 A700	BD Biosciences	560566
CD34 PE-CY7	BD Biosciences	348791
CD11b APC	BD Biosciences	340546
Lineage cocktail FITC	BD Biosciences	340937
Bacterial and Virus Strains		
Max efficiency DH5alpha competent cells	ThermoFisher	18258012
Biological Samples		
Human Cord blood samples	University of Colorado Hospital	N/A
Mobilized adult BM mononuclear cells	University of Colorado Hospital	N/A
Primary AML samples	University of Colorado Hospital	N/A
Chemicals, Peptides, and Recombinant Proteins		
APOCYNIN	Sigma-Aldrich	178385
DPI	Sigma-Aldrich	43088
Cell-ROX deep red	Life technologies	C10422
dsTat-Scramble	Ana-spec	AS-63821
dsTat-gp91	Ana-spec	AS-63821
4-OHT	Sigma-Aldrich	H7904
Tamoxifen	MP Biomedical	0215673883
Rotenon	Sigma-Aldrich	R8875
Oligomycin A	Sigma-Aldrich	871744
Antimycin	Sigma-Aldrich	A8774
RIPA lysis buffer	Thermo Fisher	89900
Halt Protease inhibitor	Thermo Fisher	87785
Laemmli sample buffer	BioRad	1610737
FCCP	Sigma-Aldrich	C2920
May-Grunwald stain	Sigma-Aldrich	MG500
Geimsa stain	Sigma-Aldrich	GS500
Palmitic Acid, [9,10-^{3}H(N)]-, 1mCi (37MBq) Radiolabeled	PerkinElmer	NET043001MC
Palmitic Acid	Sigma-Aldrich	P0500-100G

Author Manuscript Author Manuscript Author Manuscript Author Manuscript

REAGENT or RESOURCE	SOURCE	IDENTIFIER
Deposited Data		
RNaseq of WT and NOX2 KO LSCs	This paper	GEO: GSE117657
Experimental Models: Cell Lines		
293FT Cell Line	ThermoFisher	R70007
Platinum-E (Plat-E) retroviral packaging cells	Cell Biolabs, Inc	RV-101
Experimental Models: Organisms/Strains		
B6.SJL-Ptprc^{a} Pepc^{b}/BoyJ (CD45.1) mice	Craig Jordan Lab	N/A
C57BL/6J (CD45.2) mice	The Jackson Laboratory	000664
B6.129S-*Cybb*^{tm1Din}/J i.e., NOX2 KO mice	Generous gift from Dr Eric Campbell and Dr. Lucy Gold lab	N/A
FOXC1 f/f; Ai14	Provided by Dr. Julie Siegenthaler lab	N/A
NOD.Cg-*Prkdc*^{scid} *Il2rg*^{tm1Wjl} Tg(CMV-IL3,CSF2,KITLG)1Eav/MloySzJ	Craig Jordan Lab	N/A
NOD.Cg-*Prkdc*^{scid} *Il2rg*^{tm1Wjl}/SzJ	Craig Jordan Lab	N/A
Oligonucleotides		
Please refer to Table S3		N/A
Recombinant DNA		
PLKO.1 GFP	Craig Jordan Lab	N/A
pPax2	Craig Jordan Lab	N/A
pMD2	Craig Jordan Lab	N/A
MSCV-p210BCR-ABL-IRES-GFP	Craig Jordan Lab	N/A
MSCV-NUP98-HOXA9-IRES-YFP	Craig Jordan Lab	N/A
MSCV-CRE-ERT2-PURO	Addgene	22776 (Kumar et al., 2009)
MSCV-PURO	Dr. Patricia Ernst lab	N/A
PLKO.1-shNT-Puro	CU genomics core	N/A
PLKO.1-shp22phox-Puro	CU genomics core	N/A
PLKO.1-shNT-GFP	This paper	N/A
PLKO.1-shNOX2#1-GFP	This paper	N/A
PLKO.1-shNOX2#2-GFP	This paper	N/A
PLKO.1-shFOXC1-GFP	This paper	N/A
Software and Algorithms		
Graphpad Prism 6	https://www.graphpad.com	Version 6
FlowJo	https://www.flowjo.com/	Version 10
Other		
CD34+ MicrobeadKit	Miltenyi Biotec	130-056-702
LS Columns	Miltenyi Biotec	130-042-401
Ficoll Paque	GE Healthcare	GE17-1440-02